NUMERICAL DETERMINATION OF APPARENT HORIZONS

ATHOL J KEMBALL

ABSTRACT

This Research Report is concerned with the numerical evaluation of the Nakamura algorithm (Nakamura, Kojima and Oohara 1984) for determing marginally outer trapped surfaces and apparent horizons in (3+1) numerical relativity. The algorithm is applied to three sets of time-symmetric initial data; a single shifted Schwarzschild black hole and the case of two and three collinear Schwarzschild black holes. Both initial data with and without inversion symmetry are used and the results are compared to previous work which used different numerical methods. In summary, the algorithm is well- suited to determining the position of smooth marginally outer trapped surfaces; it has exponential convergence and is robust and stable. Several modifications are introduced to improve the robustness and convergence of the algorithm. It is not, however, well-suited to determining highly distorted apparent horizons, determining apparent horizons to high accuracy or accurately determing the closed trapped region.

CONTENTS

INTRODUCTION

With the advent of modern computing power, numerical relativity has become a powerful technique for investigating realistic astrophysical problems which are not amenable to analytic solution. This includes such problems as stellar collapse and the dynamics of black hole systems. It is often important to determine when and if a black hole forms in such numerical space-times. An event horizon is non-trivial to determine as the entire future development of the space-time must be known. It is possible, however, to determine the position of an apparent horizon on a given hypersurface using only data defined on the hypersurface itself. The existence of an apparent horizon implies that there is an event horizon surrounding it or coinciding with it if the space-time obeys certain reasonable properties. Also, the area of the apparent horizon can, in some cases, be used to determine the limits for energy extraction from black hole systems.

The position of the apparent horizon on an initial data surface is defined by the trapped surface equation. This is a non-linear second order partial differential equation which is difficult to solve numerically. Various numerical methods have been proposed for solving this equation including a method by Nakamura, Kojima and Oohara (1984), which can be used in the full (3+1) formulation of numerical relativity.

This research report is concerned with the numerical evaluation of the Nakamura algorithm and an assesment of its usefulness in (3+1) numerical relativity. A reliable method for determining apparent horizons in (3+1) numerical relativity has become increasingly important as initial data become available for black hole systems with non-zero linear and angular momentum (York 1988).

Apparent horizons are known for two time-symmetric Schwarzschild black holes due to previous work by Cadez (1974) and Bishop (1982,1984) using other numer-

ical methods. These results are re-derived using the Nakamura algorithm for the purposes of comparison. The case of three collinear Schwarzschild black holes is also considered.

As a result of these examples several improvements are made to the algorithm which lead to improved stability and convergence. A review is given of the general applicability of the algorithm and its relation to other numerical methods.

The research report is structured in the following manner.

In Chapter 1 a review is presented of the initial value formulation of general relativity. This includes a dicussion of the constraint and evolution equations.

Chapter 2 discusses methods for determining initial data for black hole systems. This follows the prescription of Kulkarni, Shepley and York (1983).

In Chapter 3 the global properties of apparent and event horizons are discussed and a review is given of their importance in numerical relativity. The trapped surface equation is derived and existing numerical methods for solving the equation are discussed.

Chapter 4 is concerned with the implementation and numerical evaluation of the Nakamura algorithm. The algorithm is modified to improve the stability and convergence. Apparent horizons are determined for two time-symmetric Schwarzschild black holes described by both the Misner (1963) and Misner and Wheeler (1957) initial data. The results for this system obtained by Bishop (1982) and Smarr et al. (1976) are confirmed. In addition, apparent horizons are determined for three collinear Schwarzschild black holes. In closing, the advantages and limitations of the Nakamura algorithm are summarised and a comparison is made with other numerical methods.

The following notational conventions are used:

General Latin indices are used for all tensor quantities to simplify the presentation and to emphasise a global geometric approach to the initial value formulation. An explicit (3+1) coordinate basis is introduced in deriving the trapped surface equation in section 3.3 and the notation is adapted accordingly. Greek indices with a range of 1 to 3 are thereafter used to denote space-like tensor quantities while barred Greek indices are used to cover the index range 1 to 2.

A space-time metric g_{ab} of signature (-,+,+,+) is used throughout. Tensor indices enclosed in brackets are assumed to be symmetrized i.e. $K_{(ab)} = \frac{1}{2}(K_{ab} + K_{ba})$.

CHAPTER ONE

THE CAUCHY FORMULATION OF GENERAL RELATIVITY

Introduction

In this chapter a review is given of the Cauchy formulation of general relativity. General references used are Smarr and York (1978), York (1978), Adler, Bazin and Schiffer (1975) and Misner, Thorne and Wheeler (1973). A more rigorous mathematical approach can be found in Hawking and Ellis (1973).

The importance of numerical relativity is discussed in section 1.1. In section 1.2 the constraint equations governing the choice of initial data are derived and in section 1.3 a method is discussed for their solution. The choice of kinematics is reviewed in section 1.4 and the evolution equations are derived in section 1.5.

1.1 The Importance of Numerical Relativity

The Cauchy problem in general relativity, as in other physical theories, involves the choice of initial data which uniquely determine the future evolution of the system under study. The problem can thus be formulated in terms of an initial value problem and an evolution problem. In general relativity the initial value problem concerns the choice of suitable initial data to describe the gravitational field and its sources, while the evolution problem specifies how these data are to be evolved in order to generate the full space-time geometry.

The first step in constructing initial data in general relativity involves choosing a hypersurface slicing or foliation of space-time. The foliation is usually chosen to be spacelike and this will be assumed in the ensuing discussion. Initial data

for the gravitational field are specified on a slice Σ, and then evolved to the other slices of the foliation to build up a description of the space-time. The initial data for the gravitational field on a slice, Σ, consists of the space-time metric γ_{ab}, and its first derivative normal to the slice, which is equivalently described by the extrinsic curvature of the slice, K_{ab}. First derivatives of the metric within Σ can be determined from γ_{ab}, assuming that the metric functions are suitably differentiable. The metric γ_{ab} specifies the intrinsic geometry of Σ while K_{ab} describes how the time slice is imbedded in the surrounding space-time. This will be discussed in more detail in section 1.2.

Arbitrary initial data (γ_{ab}, K_{ab}) on a hypersurface Σ do not determine a unique Cauchy evolution in terms of the Einstein field equations. This is a result of the fundamental coordinate freedom in general relativity. Consequently the initial data must satisfy a set of constraint equations on the initial hypersurface. These arise naturally from the Cauchy form of the Einstein field equations and are discussed in section 1.2d.

The first part of the evolution problem involves choosing a congruence of observer worldlines threading the foliation along which the initial data are to be evolved. The choice of hypersurface slicing and the observer worldlines constitute the kinematics of the formulation and can be freely specified in general relativity. The kinematics are usually chosen to maximise the space- time region covered by the evolution of the initial data, and to simplify the interpretation of the dynamics. This will be discussed further in section 1.4.. The full space-time geometry is thus constructed as a time history of the spatial tensor fields (γ_{ab}, K_{ab}) which are determined on each slice of the foliation. The evolution equations can be derived from the Einstein field equations in Cauchy form and are given in section 1.5.

Numerical relativity is the solution of the Cauchy problem in general relativity by computational or numerical means. This involves the numerical determination

and evolution of initial data for a given space-time. Once the space-time has been constructed numerically physical properties of interest can be extracted. These may include global properties such as the position of apparent or event horizons in the space-time.

Numerical relativity, although inferior to a knowledge of analytic solutions, can be used to address many astrophysically interesting problems such as gravitational radiation, cosmology and the N-body problem. It is non-trivial to find exact solutions for these physically realistic systems, which are typically characterised by strong gravitational fields, high speed internal motions and a lack of underlying symmetry. Analytic and numerical approaches are, however, strongly mutually supportive.

Exact solutions provide important test-bed calculations for numerical relativity (Centrella et al. 1986) and in turn numerical results may suggest useful analytic approximations (Bishop 1988). In particular, computational algebraic results sometimes suggest simpler analytic methods (MacCallum 1986). The sensitivity of the numerical solution to important physical parameters can be determined empirically and often leads to enhanced physical intuition (Schutz 1986).

Complex numerical calculations are possible with modern computing power, which has greatly expanded the scope of numerical relativity. Numerical solutions are determined using the full non-linear Einstein field equations and are thus not approximate in the weak-field sense. Numerical relativity can also be used to investigate the global properties of the resulting spacetimes such as the position of event horizons and the behaviour of singularities (Eardley 1978).

1.2 The Initial Value Equations

In this section the choice of space-time foliation is discussed and the equations

which constrain the initial data are derived.

1.2a Space-time Foliation

Space-time will be modelled as a C^∞ four-dimensional Riemannian manifold $\mathcal{M}$ with metric g_{ab}. The manifold is assumed to have connected Hausdorff topology and a Lorentz metric.

A hypersurface in $\mathcal{M}$ is defined as the image of a three-dimensional manifold $\mathcal{S}$ under an imbedding $\Theta : \mathcal{S} \rightarrow \mathcal{M}$ and is denoted by $\Theta(\mathcal{S})$ (Hawking and Ellis (1973,p44)). The map Θ induces a vector mapping $\Theta_* : T_p \rightarrow T_{\Theta(p)}$ and a one-form mapping $\Theta^* : T^*_{\Theta(p)} \rightarrow T^*_p$, where T_p is the tangent vector space and T^*_p the dual one-form space at a point $p \in \mathcal{S}$. The tangent spaces at the point $\Theta(p) \in \mathcal{M}$ are similarly denoted by $T_{\Theta(p)}$ and $T^*_{\Theta(p)}$. The induced maps are discussed in more detail by Hawking and Ellis (1973, p22). The imbedding may be defined in terms of a one-form field $\tilde{\Omega}$ where for any vector $\vec{\mathbf{X}} \in \mathcal{S}$

$$< \tilde{\Omega}, \Theta_* \vec{\mathbf{X}} >= 0 \tag{1.1}$$

The one-form field $\tilde{\Omega}$ thus defines a hypersurface slicing or foliation of space-time $\mathcal{M}$. In component form,

$$\tilde{\Omega} = \Omega_a \tilde{\mathbf{e}}^a$$

where $\tilde{\mathbf{e}}^a$ is a basis of forms on $\mathcal{M}$. The dual set of basis vectors on $\mathcal{M}$ will be denoted by $\vec{\mathbf{e}}_a$.

The one-form field $\tilde{\Omega}$ is surface-forming and closed i.e. $\mathrm{d}\tilde{\Omega} = 0$, and the hypersurfaces can be represented as level surfaces of a scalar function τ (York 1978),

$$\Omega_a = \tau_{,a} \tag{1.2}$$

A hypersurface $\Theta(\mathcal{S})$ is space-like, null or time-like if $g^{ab}\Omega_a\Omega_b$ on $\Theta(\mathcal{S})$ is less than zero, zero or greater than zero respectively. In what follows the hypersurfaces in

the foliation will be assumed to be space-like i.e $g^{ab}\Omega_a\Omega_b < 0$. Then $\tilde{\Omega}$ can be normalised in the form $\tilde{\omega} = \omega_a \tilde{e}^a$, where,

$$\omega_a = \alpha\Omega_a, \qquad g^{ab}\omega_a\omega_b = -1 \tag{1.3}$$

This implies that $g^{ab}\Omega_a\Omega_b = -\alpha^{-2}$, where α is a scalar field on $\mathcal{M}$.

The unit vector normal on each slice $\Theta(S)$ is denoted by,

$$\vec{n} = n^a \vec{e}_a$$

and is defined in terms of the condition,

$$< \tilde{\omega}, \vec{n} >= 1 \tag{1.4}$$

Therefore,

$$n^a = -g^{ab}\omega_b$$

The vector field $\vec{n}$ is tangent to the Eulerian observers of the space-time foliation. These observers are instanteously at rest in the hypersurfaces $\Theta(S)$ and have no spatial rotation.

If $\Theta(S)$ is not null then Θ_* can be extended to a map $\tilde{\Theta}_*$ (with inverse $\tilde{\Theta}^*$) of tensors of arbitrary rank on S to $\Theta(S)$ (Hawking and Ellis 1973, p45) i.e.,

$$\tilde{\Theta}_* : T^r_s[S] \rightarrow T^r_s[\Theta(S)]$$

where T^r_s denotes a tensor space of type (r,s).

The map satisfies a more general form of (1.1). For any tensor $R \in T^r_s[S]$, $\tilde{\Omega}$ has zero contraction with $\tilde{\Theta}_* R \in T^r_s[\Theta(S)]$ on any index, i.e.

$$(\tilde{\Theta}_* R)^{a_1 a_2 .. a_i .. a_j}{}_{b_1 b_2 .. b_n} \Omega_{a_i} = 0 \quad \text{,and}$$

$$(\tilde{\Theta}_* R)^{a_1 a_2 .. a_j}{}_{b_1 b_2 .. b_i .. b_n} g^{b_i c} \Omega_c = 0$$

This subset of tensors in $T^r_s[\Theta(S)]$ will be denoted by $H^r_s[\Theta(S)]$.

Thus tensors in T^r_s on S can be identified with tensors in H^r_s on $\Theta(S)$ if they correspond under the maps $\tilde{\Theta}_*$ and $\tilde{\Theta}^*$. A full discussion can be found in Hawking and Ellis (1973).

1.2b The Initial Data (γ_{ab}, K_{ab})

The the space-time metric g on $\mathcal{M}$ induces a metric $\Theta^* \mathbf{g}$ on S via the mapping $\Theta^* : T^*_{\Theta(p)} \rightarrow T^*_p$. This is defined by the condition (Hawking and Ellis (1973,p44)),

$$\Theta^* \mathbf{g}(\vec{\mathbf{X}}, \vec{\mathbf{Y}}) = \mathbf{g}(\Theta_* \vec{\mathbf{X}}, \Theta_* \vec{\mathbf{Y}}), \qquad \text{where } \vec{\mathbf{X}}, \vec{\mathbf{Y}} \in T_p, \quad p \in S$$

Now $\Theta^* \mathbf{g}$ can be mapped to $\Theta(S)$ by $\tilde{\Theta}_*$, yielding the three-metric on $\Theta(S)$,

$$\gamma_{ab} = g_{ab} + n_a n_b \tag{1.5}$$

This describes the intrinsic geometry of the hypersurface S. In mixed form γ_{ab} is a projection operator (i.e. $\gamma^a{}_b \gamma^b{}_c = \gamma^a{}_c$) and can be used to project any tensor $T \in T^r_s[\Theta(S)]$ into its tensor part T' lying in $H^r_s[\Theta(S)]$. For any T,

$$(T')^{c_1 c_2 .. c_j}{}_{d_1 d_2 .. d_n} = T^{a_1 a_2 .. a_j}{}_{b_1 b_2 .. b_n} \gamma^{c_1}{}_{a_1} \gamma^{c_2}{}_{a_2} .. \gamma^{c_j}{}_{a_j} \gamma^{b_1}{}_{d_1} \gamma^{b_2}{}_{d_2} .. \gamma^{b_n}{}_{d_n} \tag{1.6}$$

In what follows a hypersurface element of the foliation will be denoted by Σ. The spatial metric γ_{ab} defines the intrinsic geometry of Σ. It is also neccessary, however, to specify the imbedding of the hypersurface in the enveloping four-geometry $\mathcal{M}$. This is defined by the extrinsic curvature of Σ, which is given by (York 1978),

$$K_{ab} = -\gamma^c{}_a \gamma^d{}_b n_{(c;d)} \tag{1.7}$$

This can be expressed in terms of the kinematic decomposition of the covariant derivative of the time-like vector field $\vec{n}$ (Kramer et al. (1980, p77)).

$$K_{ab} = -\sigma_{ab} - \frac{1}{3}\gamma_{ab}\theta \tag{1.8}$$

where σ_{ab} is the shear tensor and θ is the expansion as measured in the local rest frame of the Eulerian observers.

K_{ab} can thus be equivalently interpreted as measuring the deformation of a surface in Σ when carried forward a unit interval of proper time normal to the hypersurface. The extrinsic curvature can also be viewed as determining the change in the unit normal $\vec{n}$ on parallel transport with respect to the enveloping four-geometry from point to point in Σ (Misner, Thorne and Wheeler (1973, p511)).

It can easily be shown that,

$$K_{ab} = -\frac{1}{2}\mathcal{L}_{\vec{n}}\gamma_{ab} \tag{1.9}$$

where $\mathcal{L}_{\vec{n}}$ denotes the Lie derivative along the vector field $\vec{n}$.

The gravitational field on an initial slice Σ is thus described by the initial data set (γ_{ab}, K_{ab}). These are spatial tensor fields defined on Σ and do not depend on the evolution away from the slice. Both tensor fields are space-like i.e. $\gamma_{ab}n^a = K_{ab}n^a = 0$.

If $K_{ab} = 0$ then the hypersurface Σ is time-symmetric (momentarily static). This implies that there is an isometry that reverses the direction of the normal $\vec{n}$ on Σ (Hawking 1972a). The initial data surface for a rotating system is thus time-asymmetric.

1.2c The Gauss-Codacci Equations

These equations provide a relation between the curvature tensors on $\mathcal{M}$ and Σ and the extrinsic curvature of Σ. This allows a simpler formulation of the constraint equations, which will be derived in the next section.

The induced metric γ_{ab} on Σ (1.5) defines a connection on Σ. Covariant differentiation with respect to this connection in Σ will be denoted by a vertical bar and is defined by (Hawking and Ellis (1973,p46)),

$$T^{a_1 a_2 .. a_j}{}_{b_1 b_2 .. b_n | c} = T^{d_1 d_2 .. d_j}{}_{e_1 e_2 .. e_n ; m} \gamma^{a_1}{}_{d_1} \gamma^{a_2}{}_{d_2} .. \gamma^{a_j}{}_{d_j} \gamma^{e_1}{}_{b_1} \gamma^{e_2}{}_{b_2} .. \gamma^{e_n}{}_{b_n} \gamma^{m}_{c} \tag{1.10}$$

where ; denotes covariant differentiation with respect to g_{ab} in $\mathcal{M}$.

In what follows the Riemann tensor and Ricci tensor defined on $\mathcal{M}$ in terms of g_{ab} are denoted by $R^{e}{}_{fgk}$ and R_{ef} respectively. The covariant derivative with respect to γ_{ab} defines a curvature tensor $R'^{a}{}_{bcd}$ on Σ in the usual way. For any vector $Y^b \in \Sigma$,

$$R'^{a}{}_{bcd} Y^b = Y^a{}_{|dc} - Y^a{}_{|cd}$$

On using (1.10) this leads to Gauss' equation,

$$R'^{a}{}_{bcd} = R^{e}_{fgk} \gamma^{a}{}_{e} \gamma^{f}{}_{b} \gamma^{g}{}_{c} \gamma^{k}{}_{d} - K^{a}{}_{c} K_{bd} + K^{a}{}_{d} K_{bc} \tag{1.11}$$

The Codacci equation can be derived from a similar use of (1.10),

$$(K^{a}{}_{b})_{|c} = (n^{d}{}_{;e} \gamma^{f}{}_{d} \gamma^{e}{}_{g})_{;h} \gamma^{a}{}_{f} \gamma^{g}{}_{b} \gamma^{h}{}_{c}$$

and is given by,

$$K^{a}{}_{b|a} - K^{a}{}_{a|b} = R_{ef} n^{f} \gamma^{e}{}_{b} \tag{1.12}$$

A full derivation of the Gauss-Codacci relations can be found in Hawking and Ellis (1973,p47) and Wald (1984,p258).

1.2d The Constraint Equations

As discussed in section 1.1, the initial data (γ_{ab}, K_{ab}) cannot be freely specified on Σ but must satisfy constraint equations. These can be derived from the Einstein field equations on Σ which do not contain terms describing the second derivative of the metric normal to Σ (Adler, Bazin and Schiffer (1975, p280); Smarr and York (1978)). This yields four relations on Σ:

$$n^c \gamma^{ab} G_{bc} = n^c \gamma^{ab} T_{bc} \tag{1.13}$$

$$n^c n^d G_{cd} = n^c n^d T_{cd} \tag{1.14}$$

where G_{ab} is the Einstein tensor and T_{ab} is the energy-momentum tensor.

The Eulerian observers measure a momentum density j^a and an energy density ρ in their local rest space, which are defined in the usual way,

$$j^a = n^c \gamma^{ab} T_{bc} \tag{1.15}$$

$$\rho = n^c n^d T_{cd} \tag{1.16}$$

Equations (1.13) and (1.14) can be simplified using the Gauss-Codacci relations (Wald (1984,p258)). Using (1.12) and (1.15), equation (1.13) becomes,

$$K^a{}_{b|a} - K^a{}_{a|b} = j_b \tag{1.17}$$

Equation (1.11) can be contracted to yield:

$$R' = R^e{}_{fgk} \gamma^g{}_e \gamma^{fk} - (K^a{}_a)^2 + K_{ab} K^{ab} \tag{1.18}$$

where R' is the scalar curvature on Σ with respect to γ_{ab}. Using (1.5) $R^e{}_{fgk} \gamma^g{}_e \gamma^{fk}$ can be expanded as:

$$R^{e}{}_{fgk}\gamma^{g}{}_{e}\gamma^{fk} = R + 2R_{ab}n^{a}n^{b}$$

$$= 2G_{ab}n^{a}n^{b} \tag{1.19}$$

where R is the scalar curvature on $\mathcal{M}$ with respect to g_{ab}.

Using (1.16),(1.18) and (1.19), equation (1.14) can be written in the form (Wald (1984,p258)):

$$R' - K_{ab}K^{ab} + (K^{a}{}_{a})^{2} = 2\rho \tag{1.20}$$

Equations (1.17) and (1.20) constitute the initial value equations on Σ which must be satisfied by $(\gamma_{ab}, K_{ab}; \rho, j_{a})$. These equations are referred to as the momentum and Hamiltonian constraints respectively. If the constraint equations hold on an initial slice Σ then they will always be satisfied in the future Cauchy development of Σ. This result follows from the Bianchi identity (York and Piran 1982, and Adler, Bazin and Schiffer 1975). Methods of solving the constraint equations will be discussed further in the next section.

1.3 The Solution of the Constraint Equations

The constraint equations (1.17) and (1.20) can be written in the form (Bowen and York 1980):

$$(K^{ab} - \gamma^{ab}trK)_{|b} = j^{a} \tag{1.21}$$

$$R' - K_{ab}K^{ab} + (trK)^{2} = 2\rho \tag{1.22}$$

These equations are most easily solved by introducing a conformal transformation of the initial data $(\gamma_{ab}, K_{ab}; \rho, j^{a})$. The conformal transformation of the three-metric is given by,

$$\gamma_{ab} = \psi^{4}\hat{\gamma}_{ab} \tag{1.23}$$

where ψ is the conformal factor ($\psi > 0$) and $\hat{\gamma}_{ab}$ is the metric of the background space. The initial value problem can be considerably simplified by this technique, particularly if a flat background space is used.

The extrinsic curvature K^{ab} is symmetric and can be split up into trace and trace-free parts,

$$K^{ab} = E^{ab} + \frac{1}{3}\gamma^{ab} trK \tag{1.24}$$

The trace-free part E^{ab} will be subjected to a conformal transformation while trK will be treated as a given scalar function (York 1978). If E^{ab} is conformally transformed as,

$$E^{ab} = \psi^m \hat{E^{ab}} \tag{1.25}$$

where $\hat{E^{ab}}$ is given, then

$$E^{ab}{}_{|b} = \psi^m \hat{E^{ab}}{}_{\|b} + (m+10)\psi^{m-1}\psi_{,b}\hat{E^{ab}} \tag{1.26}$$

where double vertical bars denote covariant differentiation with respect to the background metric $\hat{\gamma}_{ab}$ and a comma denotes partial differentiation. Indices on tensors in the background space are raised and lowered with $\hat{\gamma}_{ab}$. The tranformation (1.25) can thus be equivalently expressed as,

$$E_{ab} = \psi^{m+8}\hat{E}_{ab} \tag{1.27}$$

Equation (1.26) suggests that $m = -10$ is a simplifying choice in (1.25). Then,

$$E^{ab}{}_{|b} = \psi^{-10}\hat{E}^{ab}{}_{\|b}$$

This term occurs in the momentum comstraint equation (1.21) and motivates a conformal transformation for j^a as,

$$j^a = \psi^{-10}\hat{j}^a$$

where $\hat{j}^a$ is given.

The momentum constraint (1.21) then becomes,

$$\hat{E^{ab}}_{\|b} = \hat{j}^a + \frac{2}{3}\psi^6 (trK)^{\|a} \tag{1.28}$$

The dominant energy condition $\rho^2 - \gamma_{ab} j^a j^b > 0$ (Hawking and Ellis (1973), p91) is satisfied for all $\psi > 0$ if the energy density is conformally transformed as $\rho = \psi^{-8}\hat{\rho}$, where $\hat{\rho}$ is assumed to be given. Then (York 1978),

$$\rho^2 - \gamma_{ab} j^a j^b = \psi^{-16}(\hat{\rho}^2 - \hat{\gamma}_{ab}\hat{j}^a\hat{j}^b)$$

From (1.23) the transformation of the scalar curvature R' on Σ can be obtained as (York and Piran 1982),

$$R' = \hat{R}'\psi^{-4} - 8\psi^{-5}\hat{\nabla}^2\psi$$

where $\hat{\nabla}^2\psi = (\psi^{\|a})_{\|a}$ The conformal form of the Hamiltonian constraint (1.22) is therefore given by,

$$-8\hat{\nabla}^2\psi = 2\psi^{-3}\hat{\rho} - \hat{R}'\psi + \psi^{-7}\hat{E}_{ab}\hat{E^{ab}} - \frac{2}{3}\psi^5 (trK)^2 \tag{1.29}$$

If maximal slicing (trK=0) is chosen then the conformally transformed constraint equations (1.28) and (1.29) are uncoupled. These equations need to be supplemented by boundary conditions at spatial infinity or on any inner boundaries which may exist in the physical system under study. This will be shown more clearly in deriving initial data for black hole systems in chapter 2.

1.4 The Choice of Kinematics

This section discusses the choice of observer worldlines along which the initial data are to be evolved.

1.4a The Time Congruence

The hypersurface slicing or foliation of space-time $\mathcal{M}$ is defined by the one-form field $\tilde{\omega}$ (1.3). To complete the description of the kinematics it is also neccessary to specify a time congruence threading the slices along which the initial data are to be integrated. This time congruence defines the coordinate observers, whose worldines are permanently labelled by the spatial coordinates they acquire in the initial slice. The four-velocity vector field tangent to the coordinate observers will be denoted by $\vec{\mathrm{t}} = t^a \vec{\mathrm{e}}_a$. This can be defined in terms of the Eulerian congruence $\vec{\mathrm{n}}$ as (Smarr and York 1978),

$$t^a = \alpha n^a + \beta^a, \qquad \beta^a n_a = 0 \tag{1.30}$$

where α is the lapse function (defined in (1.3)) and β^a is the spatial shift vector. Note that $\vec{\mathrm{t}}$ also satisfies (1.4) as does $\vec{\mathrm{n}}$ i.e. $< \tilde{\omega}, \vec{\mathrm{t}} >= 1$. The vector field $\vec{\mathrm{t}}$ is restricted to be nowhere tangent to the slices Σ.

The relation between $\vec{\mathrm{t}}$ and $\vec{\mathrm{n}}$ on two neighbouring slices $\Sigma(\tau)$ and $\Sigma(\tau + \Delta\tau)$, where the slices have been parametrized by the scalar function τ, is shown in Fig. 1.1. The lapse function α is the orthogonal proper time interval between the slices. Thus $\Sigma(\tau + \Delta\tau)$ can be defined as the set of points reached from $\Sigma(\tau)$ on advancing an interval of proper time $\alpha(\Delta\tau)$ along $\vec{\mathrm{n}}$. Advancing a distance $\Delta\tau$ along the coordinate congruence $\vec{\mathrm{t}}$ defines the point in $\Sigma(\tau + \Delta\tau)$ which has the same coordinates as the base point of $\vec{\mathrm{n}}$ in Σ. This involves a spatial translation $(\Delta\tau\beta^a)$ which is defined by the shift vector as each point.

The kinematics of the formulation (α, β^a), which can be freely specified, are usually chosen to maximise the region of the Cauchy development covered by the evolution of the initial data. It is also neccessary to reduce coordinate effects in the evolution to simplify the interpretation of the dynamics. This includes the

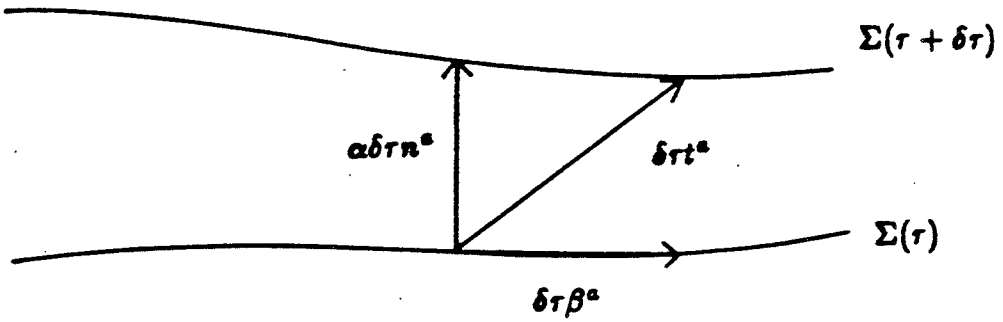

Fig. 1.1 Schematic representation of the lapse function α and shift vector β^a. The unit normal to $\Sigma(\tau)$ is $\vec{n}$, while $\vec{t}$ is tangent to the coordinate observers.

avoidance of coordinate singularities (Smarr and York 1978). Various approaches to this problem are briefly discussed in the next two sections.

1.4b The Choice of Time Slices

Minkowski space-time admits an everywhere time-like Killing vector field which suggests a natural time slicing or foliation. In general dynamical space- times there is no such prescription.

One simple approach is to choose an initial time slice and set the lapse function $\alpha = 1$ everywhere. This is known as geodesic slicing and has several disadvantages. In the future evolution of the data the Eulerian observers are focused by attractive gravitational forces, severely resticting the region of the Cauchy development covered by the slicing. From (1.8) it can be seen that the expansion θ of the Eulerian observers is given by,

$$\theta = -K^a{}_a = -trK$$

To avoid the disadvantages of geodesic slicing set,

$$trK = \mathcal{L}_{\vec{t}} trK = 0 \tag{1.31}$$

This ensures that the Eulerian observers do not converge, and defines the choice of slicing known as maximal slicing. This usually covers a larger region of the Cauchy development. Proving the existence of maximal spacelike slices is non-trivial, but they are known to exist for Minkowski, Schwarzschild and Kerr space-times, amongst others. Further details can be found in Smarr and York (1978).

1.4c The Choice of Shift Vector β^a

The shift vector β^a completes the specification of the coordinate observers once a time-slicing has been defined. The shift vector is equivalent to a three-dimensional

coordinate transform on each point in the slice Σ and can be used to reduce spurious coordinate effects in the evolution of the initial data.

The Eulerian observers $\vec{n}$ have an associated strain tensor θ_{ab}, defined by equations (1.7) and (1.8),

$$\theta_{ab} = -K_{ab} = \sigma_{ab} + \frac{1}{3}\gamma_{ab}\theta \tag{1.32}$$

Thus in a maximal slicing of space-time ($trK = -\theta = 0$) with zero shift vector β^a, the coordinate observers may have non-zero shear ($\sigma_{ab} \neq 0$). This coordinate shear may mask the underlying dynamics in the evolution. This effect, however, can be reduced by a suitable choice of β^a.

It is first neccessary to introduce a strain related tensor Φ_{ab} associated with the time-congruence. This can be defined analogously to (1.9) as (Smarr and York 1978),

$$\Phi_{ab} = \perp \mathcal{L}_{\vec{t}}\gamma_{ab}$$

where $\perp$ denotes projection into Σ as in (1.6). This is not a true strain tensor for the time-congruence as the projection in not orthogonal to $\vec{t}$. A tensor Ψ_{ab} representing the shear of the coordinate observers, can be similarly introduced as in (1.8),

$$\Psi_{ab} = \Phi_{ab} - \frac{1}{3}\gamma_{ab}tr\Phi$$

A shift vector β^a chosen to minimise Ψ_{ab} is known as a minimal distortion shift vector and satisfies the condition,

$$\gamma^{cb}\Psi_{ab|c} = 0 \tag{1.33}$$

A more complete discussion can be found in Smarr and York (1978).

The instantaneous kinematics (α, β^a) are thus defined by a set of coordinate conditions on each slice of the foliation. In the case of maximal slicing and a minimal

distortion shift vector the kinematic conditions are given by (1.31) and (1.33). In general the kinematic conditions define a coupled system of equations for (α, β^a). Boundary conditions may be imposed at spatial infinity and on any inner boundaries such as matter surfaces or event horizons. Further details can be found in York (1978) and O'Murchadha and York (1974).

1.5 The Evolution Equations

These give the evolution of (γ_{ab}, K_{ab}) along the time-congruence $\vec{t}$. In first order form they are given by (Smarr and York 1978),

$$\mathcal{L}_{\vec{t}}\gamma_{ab} = -2\alpha K_{ab} + \mathcal{L}_{\vec{\beta}}\gamma_{ab} \tag{1.34}$$

$$\mathcal{L}_{\vec{t}}K_{ab} = -\alpha_{|ab} + \alpha[R'_{ab} + (trK)K_{ab} - 2K_{ac}K^{c}{}_{b} - (S_{ab} - \frac{1}{2}\gamma_{ab}trS) - \frac{1}{2}\rho\gamma_{ab}] + \mathcal{L}_{\vec{\beta}}K_{ab} \tag{1.35}$$

where R'_{ab} is the Ricci tensor on Σ with respect to γ_{ab} and S_{ab} is the stress density measured by the Eulerian observers i.e. $S_{ab} = \gamma^{c}{}_{a}\gamma^{d}{}_{b}T_{cd}$. Equation (1.34) can be derived from the kinematic relation $\mathcal{L}_{\vec{t}} = \mathcal{L}_{\alpha\vec{n}} + \mathcal{L}_{\vec{\beta}}$ while (1.35) is a projection of the Einstein field equations into Σ (York 1978),

$$\gamma^{c}{}_{a}\gamma^{d}{}_{b}G_{cd} = \gamma^{c}{}_{a}\gamma^{d}{}_{b}T_{cd}$$

Evolution equations for the matter variables $\mathcal{L}_{\vec{t}}\rho$ and $\mathcal{L}_{\vec{t}}\vec{j}$ can be derived from projections of the energy momentum conservation equations $T^{ab}{}_{;b} = 0$ (York 1978). The evolution equations for the stress density $\mathcal{L}_{\vec{t}}S_{ab}$, however, depend on the equation of state and dynamics of the matter sources (York 1978).

CHAPTER TWO

INITIAL DATA FOR BLACK HOLE SYSTEMS

Introduction

This chapter discusses methods for constructing initial data for black hole systems. Comprehensive reviews of this problem for black hole systems can be found in Bowen and York (1980), York (1984) and Rauber (1986). Only the relevant results will be summarised here.

Section 2.1 provides a summary of initial data for single black holes and introduces the concept of inversion-symmetric initial data on an Einstein- Rosen manifold. In section 2.2 this is extended to the case of multiple black holes. Both momentarily static and dynamic black holes are considered.

2.1 Single Black Holes

2.1a Single Schwarzschild Black Hole

The Schwarzschild space-time representing a single, uncharged, non-rotating black hole is a useful starting point in discussing initial data for black hole systems. The line element in Schwarzschild coordinates (t, r, θ, ϕ) is given by,

$$ds^2 = -\left(1 - \frac{2M}{r}\right) dt^2 + \frac{dr^2}{1 - \frac{2M}{r}} + r^2 \left(d\theta^2 + \sin^2\theta d\phi^2\right) \qquad (2.1)$$

The space-time can be analytically extended by transforming to isotropic coordi-

nates $(t, \bar{r}, \theta, \phi)$,

$$t = t, \quad r = \bar{r}(1 + \frac{M}{2\bar{r}})^2, \quad \theta = \theta, \quad \phi = \phi \tag{2.2}$$

The line element (2.1) then becomes (Misner, Thorne and Wheeler (1973,p840)),

$$ds^2 = -\left(\frac{1 - \frac{M}{2\bar{r}}}{1 + \frac{M}{2\bar{r}}}\right)^2 dt^2 + \left(1 + \frac{M}{2\bar{r}}\right)^4 (d\bar{r}^2 + \bar{r}^2(d\theta^2 + \sin^2\theta d\phi^2))$$

The three-metric γ_{ab} of a space-like hypersurface $\Sigma(t)$ is given by,

$$ds_\Sigma^2 = \left(1 + \frac{M}{2r}\right)^4 (dr^2 + r^2(d\theta^2 + \sin\theta^2 d\phi^2)) \tag{2.3}$$

where, for convenience, the notation r is used in place of $\bar{r}$. The hypersurface is conformally flat and time-symmetric ($K_{ab} = 0$). The geometric structure of the hypersurface can be more clearly understood by considering an embedding of $\Sigma(t)$ in flat Euclidean three-space (Misner, Thorne and Wheeler (1973, p615)), which is shown in Fig. 2.1. The geometry consists of two asymptotically flat regions joined smoothly through a throat (or bridge) at $r = \frac{M}{2}$. The upper and lower sheets correspond respectively to the coordinate regions $r \to \infty$ and $r \to 0$ of the analytically extended manifold. The hypersurface is singularity and matter free and will be referred to as a Schwarzschild bridge.

The three-metric γ_{ab} is isometric under the mapping $J : E^3 - \{0\} \to E^3 - \{0\}$ defined in spherical polar coordinates as,

$$r' = J(r) = \frac{a^2}{r}, \quad \theta' = J(\theta) = \theta, \quad \phi' = J(\phi) = \phi \tag{2.4}$$

where E^3 is Euclidean three-space and $a = \frac{M}{2}$. In Cartesian coordinates, each point x is mapped to $x' = J(x)$ given by,

$$x' = \left(\frac{a}{r}\right)^2 x \tag{2.5}$$

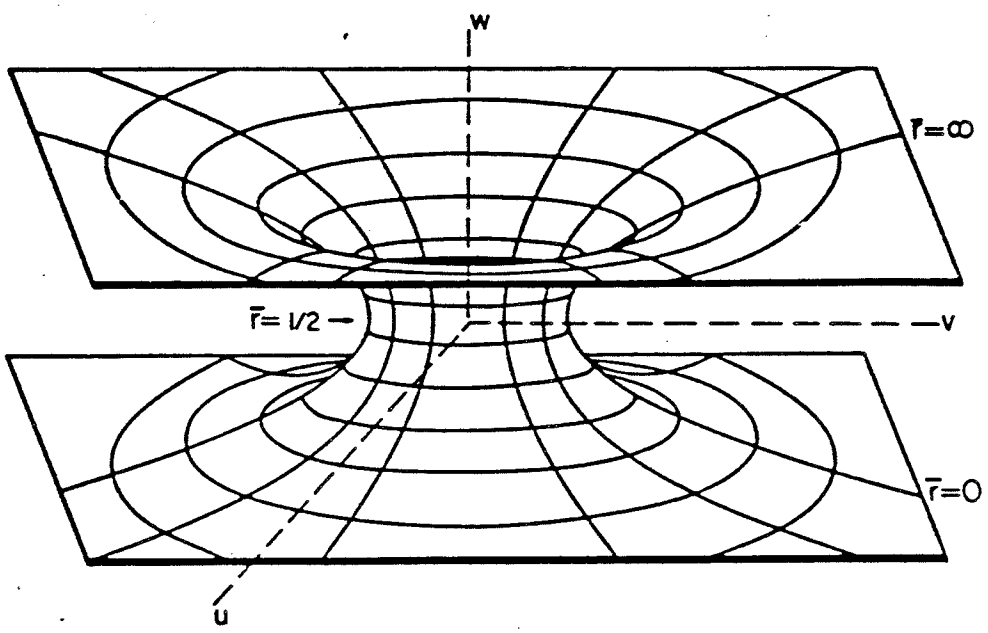

Fig. 2.1 The hypersurface (t=constant) for a single Schwarzschild black hole embedded in Euclidean three-space. The orthogonal axes are denoted by (u,v,w) (taken from Misner (1963)).

where $r = |x|$. The isometry condition can be expressed as,

$$\gamma_{ab}(x) = \gamma_{a'b'}(x') \tag{2.6}$$

The mapping (2.4) is an inversion map through the throat $r = \frac{M}{2}$ of points x on the upper sheet to points $J(x)$ on the lower sheet. The surface $r = \frac{M}{2}$ is invariant under the mapping (2.4), and thus by Lemma 1 of Gibbons (1972) is an extremal surface. In the case of a Schwarzschild black hole, direct calculation shows that the surface is minimal.

The isometry condition can be extended by requiring physical equivalence between all geometric data on the upper and lower sheets. This symmetry condition is expressed as (Kulkarni, Shepley and York 1983),

$$(\text{data at } x) = \pm J^*(\text{data at } J(x)) \tag{2.7}$$

where J^* is the pull-back map. This was first suggested by Einstein and Rosen (1935) and an initial hypersurface with this structure is referred to as an Einstein-Rosen bridge. Only data on one sheet need to be evolved due to the symmetry condition (2.7).

A detailed discussion of the differential structure and topology of a hypersurface with Einstein-Rosen structure can be found in Misner (1963) and Kulkarni, Shepley and York (1983). A brief outline, however, will be given here. The upper and lower sheets of the manifold can be regarded as point sets in a Euclidean three-space with a sphere of radius a removed. The upper and lower sheets, Y and Z respectively, are defined as,

$$Y = Z = \{p \in E^3 : |p| > a\}$$

The boundary of the sphere is represented by the point set B,

$$B = \{p \in E^3 : |p| = a\}$$

The coordinate map covering the manifold will be denoted by ξ. The range of $\xi : (\mathrm{Y\ U\ B\ U\ Z}) \rightarrow E^3$ will be described in terms of the sets,

$$X = \{x \in E^3 : |x| > a\}, \quad S = \{x \in E^3 : |x| = a\}, \quad I = J[X]$$

where J is defined in (2.5). The map ξ then takes the form (Kulkarni 1984),

$$\begin{aligned} \xi(p) = &(p^1, p^2, p^3) \in (\mathrm{X\ U\ S}) \qquad \text{if } p \in (\mathrm{Y\ U\ B}) \\ &J(p^1, p^2, p^3) \in I \qquad\quad \text{if } p \in Z \end{aligned} \tag{2.8}$$

Initial data thus need to be specified on the set (X U S U I). The geometric structure of the Einstein-Rosen hypersurface $\Sigma(t)$ provides important supplementary boundary conditions which can be used when solving the initial value problem. The constraint equations (1.28) and (1.29) on a conformally flat, time-symmetric, vacuum initial hypersurface such as $\Sigma(t)$ reduce to,

$$\hat{\nabla}^2 \psi = 0 \tag{2.9}$$

For a conformally flat metric the isometry condition (2.6) implies,

$$\psi(x) = \frac{a}{r}\psi(x') \tag{2.10}$$

Differentiating (2.10) and evaluating at $r = r' = a$, yields (Bowen and York 1980),

$$\frac{\partial \psi}{\partial r}(a) + \frac{1}{2a}\psi(a) = 0 \tag{2.11}$$

An additional boundary condition results from the fact that $\Sigma(t)$ is asymptotically flat,

$$\psi \rightarrow 1 \text{ as } r \rightarrow \infty, \quad \psi > 0 \tag{2.12}$$

The known initial data on $\Sigma(t)$ given by the metric (2.3) satisfy equation (2.9) and are consistent with the boundary conditions (2.11) and (2.12). This suggests

that initial data for more complicated black hole systems can be constructed via a similar route i.e. as conformally flat initial data on an Einstein-Rosen manifold with inversion symmetry. This will be shown more clearly in the sections that follow.

2.1b The Shifted Schwarzschild Black Hole

The three-metric of a spacelike hypersurface (t=constant) for a shifted Schwarzschild black hole in isotropic coordinates is given by Nakamura, Kojima and Oohara (1984) as,

$$ds^2 = (1 + \frac{M}{2R})^4 (dr^2 + r^2(d\theta^2 + \sin^2\theta d\phi^2)) \tag{2.13}$$

For a black hole located at $(r = d, \theta = \alpha, \phi = \beta)$ the term R takes the form,

$$R = [r^2 + d^2 - 2rd(\sin\theta \sin\alpha \cos(\phi - \beta) + \cos\theta \cos\alpha)]^{\frac{1}{2}} \tag{2.14}$$

Equations (2.13) and (2.14) can be derived from a simple coordinate shift of the three-metric (2.3).

2.1c Bowen-York Black Holes

Bowen and York (1980) have constructed initial data for a single, uncharged black hole with non-zero linear or angular momentum using the approach discussed in section 2.1a. The initial hypersurface Σ_{B-Y} on which the data are specified, is taken to be a conformally flat, maximal hypersurface with Einstein-Rosen differential structure and topology. As the black hole is dynamic the hypersurface is time-asymmetric $(K_{ab} \neq 0)$. Using the notation of section 1.3 the constraint equations (1.28) and (1.29) take the reduced form,

$$\hat{E}^{ab}{}_{\|b} = 0 \tag{2.15}$$

$$\hat{\nabla}^2\psi = -\frac{1}{8}\psi^{-7}\hat{E}^{ab}\hat{E}_{ab} \tag{2.16}$$

The symmetric tensor $\hat{E}^{ab}$ is transverse and traceless and can thus be expressed in longitudinal form (York 1973),

$$\begin{aligned}\hat{E}^{ab} &= (LW)^{ab} \\ &= \hat{W}^{b\|a} + \hat{W}^{a\|b} - \frac{2}{3}\eta^{ab}\hat{W}^{c}{}_{\|c}\end{aligned}$$

where η^{ab} is the Minkowski three-metric and $\hat{W}^a$ is a three- vector potential.

The momentum constraint (2.15) then becomes,

$$\hat{\nabla}^2 W^a + \frac{1}{3}(W^b{}_{\|b})^{\|a} = 0$$

This equation has been solved by Bowen (1979) using the ad hoc decomposition $W^a = V^a - \frac{1}{4}\theta^{\|a}$. The following solutions are given by Bowen (1979) and Bowen and York (1980),

$$\begin{aligned}\hat{E}^{\pm}_{ab} =& \frac{3}{2r^2}[P_a n_b + P_b n_a - (\eta_{ab} - n_a n_b)P^c n_c] \\ &\pm \frac{3a^2}{2r^4}[P_a n_b + P_b n_a + (\eta_{ab} - 5n_a n_b)P^c n_c]\end{aligned} \tag{2.17}$$

$$\hat{E}_{ab} = \frac{3}{r^3}(\epsilon_{cad}J^a n^c n_b + \epsilon_{cba}J^d n^c n_a) \tag{2.18}$$

where P^a and J^a are constant vectors which represent respectively the linear momentum and angular momentum of the black hole, as measured by observers at infinity. The three-dimensional permutation tensor is denoted by ϵ_{abc}, n^a is the unit normal of a sphere r=constant in flat space and a is the radius of inversion as defined in (2.5).

The trace-free extrinsic curvature E^{ab} (defined in (1.24)) is required to satisfy the Einstein-Rosen symmetry (2.7) on the initial hypersurface Σ_{B-Y}. This can be formulated as,

$$E^{ab} = \pm E^{a'b'}(x')$$

using the notation in (2.6). Consequently the conformally transformed extrinsic curvature $E_{ab} = \psi^{-2}\hat{E}_{ab}$ (1.27) must satisfy (Bowen and York 1980),

$$\hat{E}_{ab}(x) = \pm\left(\frac{a}{r}\right)^2 \hat{E}_{a'b'}(x') \tag{2.19}$$

The solutions (2.17) and (2.18) have this inversion symmetry and are thus suitable solutions of the momentum constraint equations on the Einstein-Rosen hypersurface Σ_{B-Y}.

The Hamiltonian constraint equation on Σ_{B-Y} is given by (2.16),

$$\hat{\nabla}^2\psi = -\frac{1}{8}\psi^{-7}\hat{E}_{ab}\hat{E}^{ab}, \quad r > a \tag{2.20}$$

The solution interior to $r = a$ is known from the inversion symmetry. The solution of (2.20) can be posed as a boundary value problem using (2.11) and (2.12). This has been solved numerically by Bowen (1984).

The surface $r = a$ is by construction an extremal surface, as discussed in section 2.1a. In the case of a Bowen-York black hole the surface is minimal. The inversion radius $a, (a > 0)$ is freely specifiable and acts as a scale parameter in the initial data (York and Piran 1982). The initial data for a single Schwarzschild black hole suggests that $2a$ may be a good estimate of the rest mass for a moving Bowen-York black hole. This is confirmed in a detailed analysis by Bowen and York (1980). The total energy of the solution can only be determined once the Hamiltonian constraint has been solved. The momenta J^a and P^a, however, can be specified as part of the initial data (Bowen and York 1980).

2.2 Time symmetric Initial Data for N Schwarzschild Black Holes

2.2a The Misner and Wheeler Solution

The case of N momentarily static Schwarzschild black holes is a useful starting point in constructing initial data for multiple black hole systems. The initial hypersurface Σ_{N_s} is time symmetric ($K_{ab} = 0$) and will be assumed to be conformally flat. Each black hole has a rest mass m_α and is located at the point c_α in E^3 ($\alpha = 1..N$). The Euclidean separation of the point x from the α-th black hole will be denoted as $r_\alpha = |x - c_\alpha|$. The separation of x from the origin is denoted by r as before. The constraint equations on Σ_{N_s} reduce to Laplace form (2.9),

$$\hat{\nabla}^2 \psi = 0 \tag{2.21}$$

where the conformal factor ψ satisfies the boundary condition (2.12),

$$\psi \to 1, \quad r \to \infty, \quad \psi > 0 \tag{2.22}$$

Before solving (2.21) it is neccessary to define a differential and topological structure for the hypersurface Σ_{N_s}. A simple approach is to concatenate the upper sheets of N Schwarzschild bridges (Fig. 2.1) while allowing the lower sheets to remain distinct. This is shown in Fig. 2.2. No inversion symmetry is enforced between the upper and lower sheets. The hypersurface then has the topology of $E^3 - \{c_\alpha\}$ and a solution to (2.21) is,

$$\psi(x) = 1 + \sum_{\alpha=1}^{N} \frac{b_\alpha}{r_\alpha} \tag{2.23}$$

where b_α is a constant. This solution was found by Misner and Wheeler (1957).

At each point c_α the geometry is that of the extended Schwarzschild metric in isotropic coordinates (as shown in Fig. 1.1) and the hypersurface consists of (N+1)

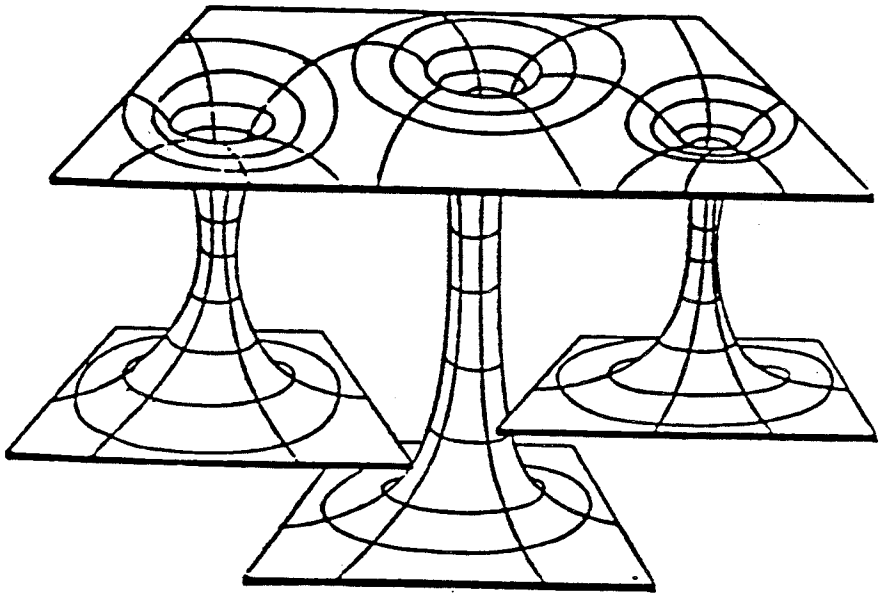

Fig. 2.2 The structure of the hypersurface Σ_{N_s} in the Misner and Wheeler solution for N time-symmetric Schwarzschild black holes (taken from Lindquist (1963)).

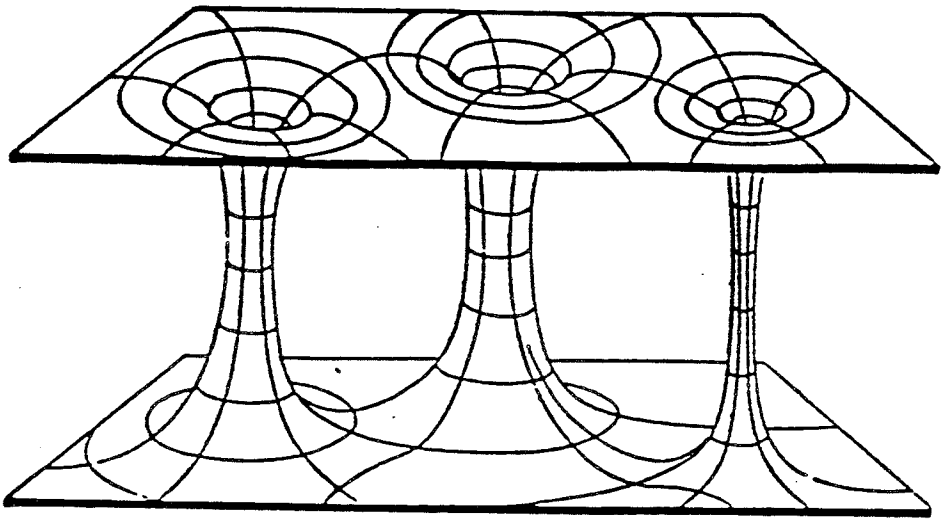

Fig. 2.3 The structure of the hypersurface Σ_{N_s} in the Misner solution for N time-symmetric Schwarzschild black holes (taken from Lindquist (1963)).

asymptotically flat sheets (Brill and Lindquist 1963). Each sheet has an associated mass energy defined in the asymptotic region (Misner, Thorne and Wheeler (1973, p452)). The upper, or (N+1)-th, sheet can be interpreted as the space in which the particles interact. The total mass energy, M_{tot}, in this sheet can be derived from (2.23) as,

$$M_{tot} = 2\sum_{\alpha=1}^{N} b_\alpha$$

This implies $b_\alpha = \frac{m_\alpha}{2}$. The mass energy M_α defined in the asymptotic region of the α-th lower sheet is given by Brill and Lindquist (1963) as,

$$M_\alpha = m_\alpha + \sum_{\alpha \neq \beta} \frac{m_\alpha m_\beta}{r_{\alpha\beta}}$$

where $r_{\alpha\beta}$ is the Euclidean separation of the α-th and β-th black holes $r_{\alpha\beta} = |c_\alpha - c_\beta|$. The difference $M_{int} = M_{tot} - \sum_{\alpha=1}^{N} M_\alpha$, represents the interaction mass energy of the system and is discussed in more detail by Gibbons (1972).

The (N+1) sheets are joined smoothly through extremal surfaces located in each Schwarzschild throat. These are deformed from spherical symmetry due to the interaction between the black holes (Brill and Lindquist 1963). Other extremal surfaces may enclose two or more black holes in the upper sheet if they are sufficiently close. This will be discussed fully in chapter 3.

2.2b The Misner Solution

This solution was derived by Misner (1963) using an initial hypersurface with full Einstein-Rosen symmetry. The hypersurface consists of two asymptotically flat sheets connected through N Einstein-Rosen bridges and is shown in Fig 2.3.

The differential structure and topology of the hypersurface is a generalisation of

that of a single Einstein-Rosen bridge discussed in section 2.1a. The upper and lower sheets of the manifold can be regarded as point sets in E^3 with N spheres of radius a_α centered at c_α removed. The upper and lower sheets, denoted by Y and Z respectively, are defined as (Kulkarni, Shepley and York 1983),

$$Y = Z = \{p \in E^3 : |p - c_\alpha| > a_\alpha, \quad \alpha = 1..N\}$$

Each sphere will be represented as the point set B_α,

$$B_\alpha = \{p \in E^3 : |p - c_\alpha| = a_\alpha, \quad \alpha = 1..N\}, \quad B = U_{\alpha=1}^{N} B_\alpha$$

The inversion map through the α-th Einstein-Rosen bridge can be generalised from (2.5) to,

$$x' = J_\alpha(x) = \left(\frac{a_\alpha}{r_\alpha}\right)^2 (x - c_\alpha) + c_\alpha, \qquad x \in E^3 - \{c_\alpha\} \tag{2.24}$$

The manifold is covered by N coordinate maps ψ_α associated with each throat. Each map ψ_α can be defined in terms its range sets in E^3. These are,

$$X = \{x \in E^3 : |x - c_\alpha| > a_\alpha, \alpha = 1..N\}$$

$$S_\alpha = \{x \in E^3 : |x - c_\alpha| = a_\alpha, \alpha = 1..N\}$$

$$I_\alpha = J_\alpha[X]$$

The map ψ_α is then defined as (Kulkarni 1984),

$$\begin{aligned} \psi_\alpha(p) = &(p^1, p^2, p^3) \in (\text{X U } S_\alpha) \quad \text{if } p \in (\text{Y U} B_\alpha) \\ &J_\alpha(p^1, p^2, p^3) \in I_\alpha \qquad \text{if } p \in Z \end{aligned} \tag{2.25}$$

The Einstein-Rosen symmetry condition which provides physical equivalence between geometric data on the upper and lower sheets, is similarly generalised as,

$$(\text{data at } x \in X) = \pm J_\alpha^*(\text{data at} J_\alpha(x)) \tag{2.26}$$

where J_α^* is the pull-back map (Kulkarni 1984). An Einstein-Rosen manifold with the above differential structure will be denoted by M_N.

Thus initial data consistent with the constraint equations need to be specified on the set $X' = U_{\alpha=1}^{N}(\mathrm{X\ U}\ S_\alpha\ \mathrm{U}\ I_\alpha)$. As can be seen from (2.25), each point $p \in Z$ on the lower sheet is covered by several coordinate maps. The symmetry condition (2.26) ensures that these overlapping maps to X' are consistent.

A solution of the Hamiltonian constraint (2.21) consistent with the symmetry condition (2.26) was found by Misner (1963). The Einstein-Rosen symmetry condition applied to the three-metric γ_{ab} requires that the conformal factor satisfies (2.10) i.e.

$$\psi(x) = (\frac{a_\alpha}{r_\alpha})\psi(J_\alpha x), \qquad x \in X' \tag{2.27}$$

These can be written as $J_\alpha[\psi](x) = \psi(x)$ where the action of J_α on ψ is given by,

$$J_\alpha[\psi](x) = (\frac{a_\alpha}{r_\alpha})\psi(J_\alpha x) \tag{2.28}$$

The boundary condition (2.22) ensures that the hypersurface is asymptotically flat; $\psi \to 1$, as $r \to \infty$. By inversion in the $\alpha - th$ sphere ψ must therefore contain a term,

$$J_\alpha[1] = \frac{a_\alpha}{r_\alpha}$$

By inversion in the β-th sphere there must also be an image term $J_\beta J_\alpha[1]$ interior to B_β. This process continues indefinitely and leads to a series solution for ψ given by (Misner 1963),

$$\psi = S[1] \tag{2.29}$$

where $S = 1 + \sum' J_{i_1} J_{i_2} .. J_{i_n}$. The summation extends over all indices ($i_k = 1..N$) subject to the condition $i_{k+1} \neq i_k$. All terms of finite length ($n \geq 1$) are included in the summation.

It is easily shown (Misner 1963) that (2.29) satisfies the inversion symmetry (2.26) between the upper and lower sheets through each and every throat, i.e.

$$J_\alpha[S] = S$$

using the notation of (2.27) and (2.28). In addition, the series (2.29) is positive, analytic and converges to a solution of the Hamiltonian constraint (2.21) in the region $X \subset X'$ (Misner 1963). The Einstein-Rosen symmetry ensures that there is a matched solution on the lower sheet.

2.2c Time-Symmetric Initial Data for N Reissner-Nordstrom Black Holes

Initial data for N Reissner-Nordstrom black holes on a surface of time- symmetry have been obtained Brill and Lindquist (1963) and Lindquist (1963), by similar methods to those used in the previous section. The addition of electric charge increases the available energy but does not qualitatively alter the nature of the solutions unless the Reissner-Nordstrom black holes become extreme ($q > m$) (Gibbons 1972).

2.2d Initial Data for N Dynamic Black Holes

Initial data for N black holes with linear or angular momentum are an important starting point in determining astrophysically realistic numerical space-times.

These data are constructed using the same strategy discussed in the preceding sections. The initial hypersurface is taken to be a conformally flat maximal Einstein-Rosen manifold M_N with the differential and topological structure defined in section 2.2 (Fig 2.3). The hypersurface is, however, time- asymmetric ($K_{ab} \neq 0$) and the constraint equations take the form (2.15) and (2.16).

The inversion symmetry of $\hat{E}_{ab}$ (2.19) can be generalised to M_N as (York 1984),

$$[Q_\alpha \hat{E}_{ab}] = \hat{E}_{ab}(x) = \pm(\frac{a_\alpha}{r_\alpha})^2 \hat{E}_{a'b'}(J_\alpha(x))$$

where Q_α is regarded as an operator. It can be shown that as $\hat{E}_{ab}$ is trace-free, symmetric and has zero divergence (2.15) then so are terms of the form $[Q_{\alpha_1} Q_{\alpha_2} .. Q_{\alpha_n} \hat{E}]_{ab}$ (York 1984; Kulkarni 1984).

Now define the inversion operator $\mathcal{Q}$ analogously to S in (2.29) as,

$$\mathcal{Q} = 1 + \sum{}' Q_{\alpha_1} Q_{\alpha_2} .. Q_{\alpha_n}$$

The summation $\sum'$ extends over all indices ($\alpha_k = 1, , N$) and includes all terms of finite length ($n \geq 1$) subject to the condition $\alpha_{k+1} \neq \alpha_k$ (Kulkarni 1984). Thus if $\hat{E}^0_{ab}$ is a solution of the momentum constraint then so is $\hat{E}_{ab} = [\mathcal{Q}\hat{E}^0]_{ab}$. In addition if ψ satisfies (2.27) then $\hat{E}_{ab}$ will satisfy the Einstein-Rosen symmetry condition (2.26) (Kulkarni 1984). The Bowen-York solution for a single black hole given by (2.17) or (2.18) can be used for $\hat{E}^0_{ab}$.

The Hamiltonian constraint has the same form as in (2.20) and is supplemented by the boundary condition (2.12). The boundary condition (2.11) takes the general form on M_N given by (Kulkarni, Shepley and York 1983),

$$\left.\frac{\partial \psi}{\partial r_\alpha}\right|_{r_\alpha = a_\alpha} + \frac{1}{2a_\alpha}\psi(a_\alpha) = 0$$

The initial value problem for N time-asymmetric black holes is not yet completely solved (York 1988). Full reviews of current work can be found in Kulkarni, Shepley and York (1983), Kulkarni (1984), Bowen, Rauber and York (1984) and Bowen (1985).

CHAPTER THREE

APPARENT HORIZONS IN NUMERICAL RELATIVITY

Introduction

In this chapter the problem of determining apparent horizons in numerical relativity is addressed. In section 3.1 apparent and event horizons are defined and their global properties discussed. The importance of apparent horizons in numerical relativity is considered in section 3.2. The trapped surface equation which is used to determine apparent horizons is derived in section 3.3 and a review of existing numerical methods used to solve this equation is given in section 3.4. Section 3.5 includes a description of the algorithm of Nakamura, Kojima and Oohara (1984) which will be evaluated more fully in chapter 4.

3.1 Global properties of Apparent Horizons and Event Horizons

A rigorous treatment of the global properties of apparent horizons and event horizons can be found in Hawking and Ellis (1973) and Hawking (1972b). Other useful references are Wald (1984) and Demianski (1985). The important results from these references are briefly summarised in this section.

Black holes may be intuitively understood as regions of space-time where the gravitational field is so strong that infalling matter or radiation, once having entered the region, can never escape. Such a region may form, for example, after the gravitational collapse of a massive body.

A more precise formulation of this concept requires that the underlying space- time manifold satisfies certain reasonable properties. In particular the manifold must be

time-orientable. This implies that it is possible to designate non-spacelike vectors as either future- or past-directed continuously at each point of the manifold, and allows a description of the causal structure of the space-time. The causal past of a point $p \in \mathcal{M}$, denoted as $J^-(p)$, is defined as the set of all events that causally precede p. An event q is said to causally precede the event p if there is at least one smooth future-directed non-spacelike curve that extends from q to p (Hawking and Ellis 1973, p183). Thus if future null infinity is denoted by $\mathcal{I}^+$, then $J^-(\mathcal{I}^+)$ defines the region in $\mathcal{M}$ from which particles or radiation can escape to infinity in the future direction.

In addition the space-time must be strongly future asymptotically predictable from a partial Cauchy surface $\Sigma(\tau)$ in $\mathcal{M}$, where a partial Cauchy surface is defined as a space-like hypersurface which is not intersected more than once by any non-spacelike curve (Hawking and Ellis 1973, p204). Future asymptotic predictability is essentially equivalent to the assumption that there are no naked singularities to the future of $\Sigma(\tau)$. A naked singularity is visible from $\mathcal{I}^+$ and violates Penrose's cosmic censor conjecture. A formal definition of future asymptotic predictability can be found in Hawking (1972b).

The black hole region in a future asymptotically predictable space $\mathcal{M}$ can then be defined as $\mathcal{B} = [\mathcal{M} - J^-(\mathcal{I}^+)]$ i.e. it is a region from which matter or radiation cannot escape to $\mathcal{I}^+$ (Wald 1984, p300). The boundary of $\mathcal{B}$ is denoted by $\partial\mathcal{B} = \dot{J}^-(\mathcal{I}^+)$ and is known as the event horizon. A black hole on a partial Cauchy surface $\Sigma(\tau)$ is defined as a connected component of the set $\mathcal{B}(\tau) = [\Sigma(\tau) - J^-(\mathcal{I}^+)]$.

The event horizon is a null surface generated by null geodesics which have no future endpoints and non-positive convergence. A black hole can thus never disappear or bifurcate. In addition the black hole area theorem of Hawking (1972b) shows that

the area of the boundary of a black hole must increase with time. This theorem holds in a regular predictable space $\mathcal{M}$ developing from a partial Cauchy surface $\Sigma(\tau)$ where all null vectors k^a satisfy the energy condition $R_{ab}k^a k^b \geq 0$. Regular asymptotic predictability is a stronger form of future asymptotic predictability and is discussed in detail by Hawking and Ellis (1973). Thus if two black holes $\mathcal{B}_1(\tau_1)$ and $\mathcal{B}_2(\tau_1)$ on a surface $\Sigma(\tau_1)$ merge to form a single black hole $\mathcal{B}_3(\tau_2)$ on the surface $\Sigma(\tau_2)$ then:

$$Area(\mathcal{B}_3) > area(\mathcal{B}_1) + area(\mathcal{B}_2) \tag{3.1}$$

Although the event horizon has several useful properties, it is not always convenient to determine in practice. The position of the event horizon on a surface $\Sigma(\tau)$ can only be determined if the entire future development of the surface is known. It is possible, however, to determine an apparent horizon in $\Sigma(\tau)$ which depends only on the initial data on the surface. This can be defined in terms of the theory of outer trapped surfaces.

Trapped surfaces are closely associated with gravitational collapse and the formation of space-time singularities. A closed trapped surface is defined as a compact spacelike two-surface without boundary where the ingoing and outgoing orthogonal null geodesics are converging (i.e. $\hat{\theta} < 0$) (Hawking and Ellis 1973, p262). An outer trapped surface is similarly defined except that only the outgoing null geodesics are required to be converging. If certain other conditions hold, the existence of a closed trapped surface implies that there is a singularity in the space-time. In addition, any outer or closed trapped surface $\mathcal{F}(\tau)$ on a partial Cauchy surface $\Sigma(\tau)$ in a regular predictable space must lie within the black hole region (i.e. $\mathcal{F}(\tau) \subset \mathcal{B}(\tau)$).

Now, the set of points in $\Sigma(\tau)$ through which there lies an outer trapped surface defines the trapped region in $\Sigma(\tau)$ (Hawking and Ellis 1973, p320). The outer

boundary of each individual connected component of the trapped region is known as a marginally outer trapped surface, as it is a two-surface where the outgoing orthogonal null geodesics have zero convergence (Proposition 9.2.9; Hawking and Ellis 1973,p321). These surfaces are topologically S^2. The apparent horizon is defined as the union of the outer boundaries of the connected components of the trapped region. From the previous discussion of closed trapped surfaces it is known that each component of the apparent horizon must lie within or coincide with a component of the true event horizon. The converse of this statement, however, is not neccessarily true.

Apparent horizons in stationary space-times have properties of particular relevance to this research. A black hole is said to be stationary if there is a Killing vector in the asymptotic region enclosing the black hole which is time-like at future and past null infinity (Demianski 1985, p182). Stationary black hole space-times are of interest as it is believed that most physically realistic black hole configurations will asymptotically approach a stationary state. The Killing vector symmetry implies that the area of a space-like cross-section of the null geodesic generators of the event horizon is independant of time. This result can be used to show that the shear and expansion of the null geodesics in the horizon must be zero. Thus the stationarity only holds if no matter or gravitational radiation crosses the horizon of the black hole. The fact that the null geodesics have zero expansion implies that the apparent and event horizons coincide for stationary black holes.

If an apparent horizon is located on a surface of time symmetry then it will be an extremal two-surface i.e. the first variation of its area is zero (Gibbons 1972). This will be discussed further in section 3.3.

3.2 The Importance of Apparent Horizons in Numerical Relativity

In problems typically treated in numerical relativity, such as gravitational collapse

and the merging of black hole systems, it is important to determine when and if the future numerical evolution of the initial data contains a black hole. The determination of an event horizon, however, requires that the future asymptotic development of the numerical space-time be known arbitrarily close to future null infinity. In practice it is not possible to evolve numerical initial data infinitely far into the future. Once singularities and event horizons have formed in the space-time, the coordinates may no longer adequately cover the region of interest. Even if the space-time geometry is determined numerically over a sufficiently large region, finding the position of the event horizon on a surface $\Sigma(\tau)$ remains a non-trivial problem. It is neccessary to follow orthogonal null geodesics starting from various points in $\Sigma(\tau)$ sufficiently far towards I^+ that it can be decided whether they lie inside or outside $\dot{J}^-(I^+)$.

The position of the event horizon $\partial\mathcal{B}(\tau) = \partial\mathcal{B} \cap \Sigma(\tau)$, which is a two-surface in $\Sigma(\tau)$, can be determined by interpolation once a sufficient number of spatially adjacent points $p, q \in \Sigma(\tau)$ have been found such that $p \in J^-(I^+), \quad q \in [\Sigma(\tau) - J^-(I^+)]$. In full (3+1) numerical relativity this will be costly in terms of computer storage and computational requirements. Event horizons have been determined numerically for the case of spherical gravitational collapse where the problem is more tractable due to the symmetry (Shapiro and Teukolsky 1979, 1980). The apparent horizons and event horizons determined numerically in this case have global properties consistent with the results of Hawking and Ellis (1973) as discussed in section 3.1.

Studies of horizons in numerical relativity can also be used to derive limits for the extraction of energy from black hole systems. Consider an initial data surface $\Sigma(\tau)$ with a black hole bounded by an event horizon $\partial\mathcal{B}(\tau)$. The Hawking black hole area theorem states that the area, A, of the event horizon must increase with time. The black hole may be considered to have an associated irreducible mass

energy M_{ir} defined by (Misner, Thorne and Wheeler 1973, p913),

$$A = 16\pi M_{ir}^2$$

This mass energy is irretrievably lost behind the event horizon and cannot be extracted by any classical general relativistic process.

The future asymptotic development of a possibly distorted black hole on $\Sigma(\tau)$ is widely believed to approach a stationary solution of the Kerr-Newman type. This process may be accompanied by the emission of gravitational radiation. If the initial surface $\Sigma(\tau)$ has a total mass energy M_{tot} defined asymptotically at spatial infinity, then the maximum interaction mass energy, M_{grav} available to be radiated in this way is given by,

$$M_{grav} = M_{tot} - M_{ir}$$

Now the area $\tilde{A}$ of an apparent horizon on $\Sigma(\tau)$ places a lower limit, $\tilde{M}_{ir}$, on the irreducible mass of the black hole.

$$\tilde{M}_{ir} = \sqrt{\frac{\tilde{A}}{16\pi}}$$

The determination of the area of an apparent horizon on $\Sigma(\tau)$ can thus be used to place an upper limit on the mass energy which may be re- distributed as gravitational radiation in the future evolution of the space- time (Gibbons and Schutz 1972). The interaction energy will also produce tidal distortion in the event horizon. Therefore the deviation of the apparent horizon from spherical symmetry provides another means of estimating the energy available as gravitational radiation (Cadez 1974).

Numerical studies of the area of apparent horizons in stationary space-times can also be used to further the understanding of the Penrose process whereby rotational

and electromagnetic mass energy can be extracted from black holes. Efficiency limits for energy extraction can be derived from the relation, $\delta M_{ir} > 0$. This is well known for the analytic Kerr-Newman solution but may need to be determined numerically for more complicated space-times such as a black hole surrounded by a rotating magnetized disk of plasma (Wagh, Dhurandhar and Dadhich 1985). Such energy extraction processes may play an important astrophysical role in powering quasars and active galactic nuclei.

3.3 The Derivation of the Trapped Surface Equation

In this section the tetrad formalism and the Newman-Penrose null tetrad are briefly reviewed, and the trapped surface equation is derived.

3.3a The Tetrad Formalism

The primary references for this section are Chandrasekhar (1983) and Stephani (1982).

It is often convenient in general relativity to specify a set of linearly independent basis vector fields on space-time which are not neccessarily derived as tangent vectors of the local coordinate congruences. This is known as a tetrad basis and will be denoted by:

$$e_{(\alpha)}{}^{p}, \qquad \alpha = 1,2,3,4 \qquad p = 0,1,2,3$$

The tetrad index in parentheses identifies each basis vector in the set and p is the usual tensor index. It is also assumed that (Chandrasekhar 1983),

$$e_{(\alpha)}{}^{p} e_{(\beta)p} = \eta_{(\alpha)(\beta)} \tag{3.2}$$

where $\eta_{(\alpha)(\beta)}$ is a constant, symmetric matrix with inverse $\eta^{(\alpha)(\beta)}$. Tensor indices are raised and lowered with the space-time metric g_{ab} while tetrad indices are

raised and lowered with $\eta_{(\alpha)(\beta)}$. For example,

$$e_{(\alpha)p} = g_{pq} e_{(\alpha)}{}^{q} \tag{3.3}$$

The dual basis $e^{(\alpha)}{}_{p}$ is defined such that,

$$e_{(\alpha)}{}^{p} e^{(\beta)}{}_{p} = \delta^{(\beta)}{}_{(\alpha)}, \qquad \text{and } e_{(\alpha)}{}^{p} e^{(\alpha)}{}_{q} = \delta^{p}{}_{q} \tag{3.4}$$

Contracting (3.3) with $e^{(\alpha)}{}_{p}$ and using (3.4), yields the important relation,

$$g_{pq} = e_{(\alpha)p} e^{(\alpha)}{}_{q} \tag{3.5}$$

The affine connection of the tetrad basis is characterised by the Ricci rotation coefficients $\gamma_{(\kappa)(\alpha)(\beta)}$, which are formed as (Chandrasekhar 1983),

$$\gamma_{(\kappa)(\alpha)(\beta)} = e_{(\kappa)}{}^{p} e_{(\alpha)p;q} e_{(\beta)}{}^{q} \tag{3.6}$$

These can be equivalently defined by,

$$e_{(\alpha)p;q} = e^{(\kappa)}{}_{p} \gamma_{(\kappa)(\alpha)(\beta)} e^{(\beta)}{}_{q} \tag{3.7}$$

Both the structure constants of the basis and the Ricci and Bianchi identities can be conveniently expressed in terms of the rotation coefficients. Further details can be found in Chandrasekhar (1983).

The rotation coefficients are anti-symmetric in the first two tetrad indices,

$$\gamma_{(\alpha)(\beta)(\kappa)} = -\gamma_{(\beta)(\alpha)(\kappa)} \tag{3.8}$$

This result follows from the fact that $[\eta_{(\alpha)(\beta)}]_{;p} = 0$ as $\eta_{(\alpha)(\beta)}$ are metric components, and the use of equations (3.2) and (3.6) (Chandrasekhar 1983).

3.3b The Newman-Penrose Null Tetrad

The Newman-Penrose formalism (Newman and Penrose 1962) is based on the null tetrad,

$$\vec{e}_{(\alpha)} = \{\vec{l}, \vec{k}, \vec{m}, \vec{m}^*\}, \qquad e_{(\alpha)}{}^p e_{(\alpha)p} = 0, \quad \alpha = 1,2,3,4 \tag{3.9}$$

where $\vec{l}, \vec{k}$ are real null vectors and $\vec{m}$ is a complex null vector with conjugate $\vec{m}^*$. The only non- zero scalar products within the pseudo-orthonormal basis are,

$$\vec{l}.\vec{k} = \vec{m}.\vec{m}^* = 1 \tag{3.10}$$

The complex null vector $\vec{m}$ can be decomposed as:

$$\vec{m} = \frac{1}{\sqrt{2}}(\vec{u} + i\vec{v}) \tag{3.11}$$

where $\vec{u}, \vec{v}$ are real space-like vectors orthogonal to each other and orthogonal to $\vec{l}$ and $\vec{k}$.

The Newman-Penrose tetrad exploits the null-cone structure of space-time and is useful in studies of black holes and null geodesic congruences. For this tetrad basis,

$$\eta_{(\alpha)(\beta)} = \begin{pmatrix} 0 & 1 & 0 & 0 \\ 1 & 0 & 0 & 0 \\ 0 & 0 & 0 & 1 \\ 0 & 0 & 1 & 0 \end{pmatrix}$$

and the dual basis $\vec{e}^{(\alpha)} = \eta^{(\alpha)(\beta)}\vec{e}_{(\beta)}$ is given by,

$$\{\vec{e}^{(\alpha)}\} = \{\vec{k}, \vec{l}, \vec{m}^*, \vec{m}\}$$

Using (3.5) the space-time metric g_{ab} is given by,

$$g_{ab} = 2l_{(a}n_{b)} + 2m_{(a}m^*_{b)}$$

In this tetrad basis the Ricci rotation coefficients are twelve complex quantities known as the spin coefficients. These will not be enumerated here but can be found in Chandrasekhar (1983, p42).

As $\vec{e}_{(4)} = \vec{m}^* = \vec{e}^*_{(3)}$ in this basis, the complex conjugate of any rotation coefficient $\gamma_{(\alpha)(\beta)(\kappa)}$ can be obtained by replacing all occurrences of the tetrad index (3) by the tetrad index (4) and vice versa. For example,

$$\gamma_{(3)(1)(4)} = \gamma^*{}_{(4)(1)(3)} \tag{3.12}$$

3.3c The Trapped Surface Equation

As discussed in section 3.1, each component of the apparent horizon on a space-like surface $\Sigma(\tau)$ is a marginally outer trapped surface. This is a closed two-surface where the convergence of the outgoing orthogonal null geodesics is zero ($\hat{\theta} = 0$).

In determining the position of a marginally outer trapped surface in $\Sigma(\tau)$ it is convenient to use a Newman-Penrose tetrad where $\vec{l}$ is chosen as the tangent vector to the outgoing null geodesics orthogonal to the two-surface. The surface is then spanned by the space-like real and imaginary parts of the complex null vector $\vec{m}$. If the outgoing null geodesics have zero expansion then,

$$\hat{\theta} = l^a{}_{;a} = 0 \tag{3.13}$$

From (3.7),

$$l^a{}_{;a} = e^{(\alpha)a}\gamma_{(\alpha)(1)(\beta)}e^{(\beta)}{}_{a}$$

Using (3.10) this becomes,

$$l^a{}_{;a} = \gamma_{(1)(1)(2)} + \gamma_{(2)(1)(1)} + \gamma_{(3)(1)(4)} + \gamma_{(4)(1)(3)} \tag{3.14}$$

Now $\gamma_{(1)(1)(2)} = 0$ as the rotation coefficients are anti-symmetric in the first two tetrad indices (3.8). Also as the vector $\vec{l}$ is geodesic (3.6) implies,

$$\gamma_{(2)(1)(1)} = l_{a;b}k^a l^b = 0$$

In the Newman-Penrose formalism the rotation coefficient $\gamma_{(3)(1)(4)}$ is denoted by the complex spin coefficient ρ. Thus (3.14) reduces to,

$$l^a{}_{;a} = \rho + \rho^*$$

where $\rho = \gamma_{(3)(1)(4)} = l_{a;b}m^a m^{*b}$ by (3.6) and ρ^* is the complex conjugate of ρ. Equation (3.13) can then be written as,

$$\Re(l_{a;b}m^a m^{*b}) = 0 \tag{3.15}$$

where $\Re$ denotes the real part. The further derivation of the trapped surface equation in this section closely follows the method of Nakamura, Kojima and Oohara (1984).

It is useful to introduce an associated unit vector basis $(\vec{n}, \vec{u}, \vec{v}, \vec{s})$ on the hypersurface $\Sigma(\tau)$. The unit normal to $\Sigma(\tau)$ is used as the time-like component of the basis, $\vec{n}$, while $(\vec{u}, \vec{v}, \vec{s})$ are space-like vectors lying in $\Sigma(\tau)$. The space-like vectors are chosen such that $(\vec{u}, \vec{v})$ are tangent to the marginally outer trapped two-surface in $\Sigma(\tau)$ and $\vec{s}$ is the space-like normal to the two-surface. This is illustrated in Fig. 3.1.

A Newman-Penrose null tetrad is now chosen based on the orthonormal tetrad. The vector $\vec{l}$ is chosen in the plane of $\vec{s}$ and $\vec{n}$ such that $l^a n_a = -1$. Using this

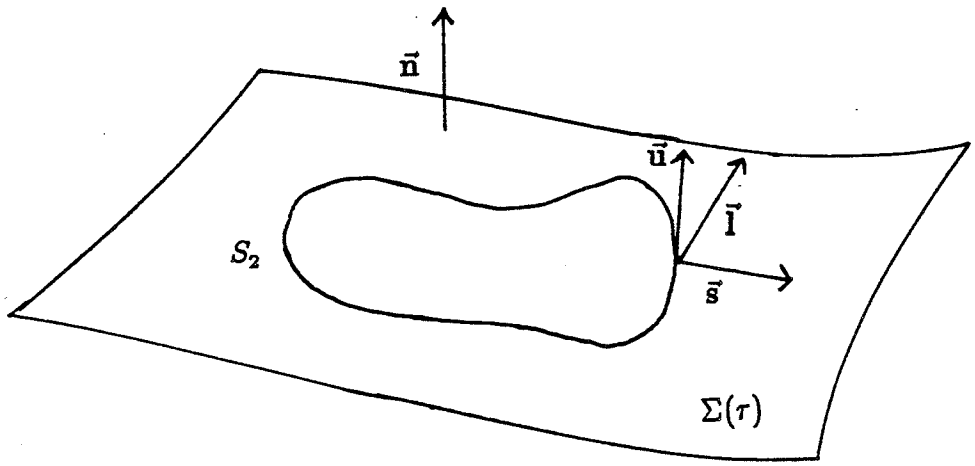

Fig. 3.1 This figure depicts the orthonormal basis used in deriving the trapped surface equation in section 3.3. One spatial dimension has been suppressed in showing a marginally outer trapped surface S_2 on an initial data surface $\Sigma(\tau)$. The unit normal to the hypersurface is $\vec{n}$ while $\vec{s}$ is the space-like normal to S_2. The surface is spanned by $\vec{u}$ (tangent vector $\vec{v}$ is suppressed) and the outgoing orthogonal null geodesic tangent vector is shown as $\vec{l}$.

and the relation (3.11), the orthonormal components are given as,

$$u^a = \frac{1}{\sqrt{2}}(m^a + \bar{m}^a)$$

$$v^a = \frac{1}{\sqrt{2}i}(m^a - \bar{m}^a) \tag{3.16}$$

$$s^a = l^a - n^a$$

The space-time metric, g_{ab}, in this orthonormal basis is,

$$g_{ab} = -n_a n_b + u_a u_b + v_a v_b + s_a s_b \tag{3.17}$$

The three-metric γ_{ab} on $\Sigma(\tau)$ is given by,

$$\gamma_{ab} = g_{ab} + n_a n_b \tag{3.18}$$

Now, from (3.16) it can be shown that,

$$\Re(m^a m^{*b}) = -\frac{1}{2}(u^a u^b + v^a v^b)$$

This can be further simplified using (3.17) and (3.18) as,

$$\Re(m^a m^{*b}) = s^a s^b - \gamma^{ab} \tag{3.19}$$

Equation (3.15) can be simplified using (3.16) and (3.19), to yield,

$$(n_{a;b} + s_{a;b})(\gamma^{ab} - s^a s^b) = 0$$

Since $\gamma^{ab} - s^a s^b$ projects into $\Sigma(\tau)$, this can be written as,

$$(\gamma^c{}_a \gamma^d{}_b n_{c;d} + \gamma^c{}_a \gamma^d{}_b s_{c;d})(\gamma^{ab} - s^a s^b) = 0$$

Using (1.7) and (1.10) this reduces to,

$$(-K_{ab} + s_{a|b})(\gamma^{ab} - s^a s^b) = 0$$

where the vertical bar denotes covariant differentiation with respect to γ_{ab} and K_{ab} is the extrinsic curvature of $\Sigma(\tau)$.

This is often given in the form (Bowen and York 1980),

$$s^a{}_{|a} = K_{ab}s^a s^b - trK \tag{3.20}$$

and is known as the trapped surface equation. If the hypersurface $\Sigma(\tau)$ is time-symmetric ($K_{ab} = 0$) then the marginally outer trapped surface is also an extremal surface, defined by $s^a{}_{|a} = 0$ (Gibbons 1972).

Now,

$$s^a{}_{|a} = s_{a|b}\gamma^{ab}$$

Using (3.18) and the orthogonality of the basis $s^a u_a = 0 = s^a v_a$, this can be written as,

$$s^a{}_{|a} = -(u^a{}_{|b}u^b s_a + v^a{}_{|b}v^b s_a)$$

and the trapped surface equation (3.20) becomes,

$$u^a{}_{|b}u^b s_a + v^a{}_{|b}v^b s_a = K_{ab}s^a s^b - trK \tag{3.21}$$

The index notation will be adapted for the remainder of the Research Report to reflect the specialised orthonormal basis $(\vec{n}, \vec{u}, \vec{v}, \vec{s})$ that has been chosen. Greek indices with a range 1,2,3 will henceforth be used for all space-like vectors and tensors lying in $\Sigma(\tau)$.

Each marginally outer trapped surface is a two-surface in $\Sigma(\tau)$ and can thus be expressed as,

$$x^\alpha = x^\alpha(\epsilon, \mu) \tag{3.22}$$

where ϵ, μ parametrise the surface. The tangent vectors to the two- surface $(\vec{p}, \vec{q})$ are given in the usual way as,

$$p^\alpha = \frac{\partial x^\alpha}{\partial \epsilon}, \qquad q^\alpha = \frac{\partial x^\alpha}{\partial \mu}$$

These vectors can be expressed linearly in terms of the orthonormal tangent vectors u^α and v^α in the form,

$$\begin{aligned} u^\alpha &= a_1 p^\alpha \\ v^\alpha &= a_2 p^\alpha + a_3 q^\alpha \end{aligned} \tag{3.23}$$

Applying the conditions $u^\alpha u_\alpha = v^\alpha v_\alpha = 1$ and $u^\alpha v_\alpha = 0$, yields,

$$\begin{aligned} a_1 &= B^{-0.5} \\ a_2 &= -(a_3)(a_1)^2 C \\ a_3 &= [A - \frac{C^2}{B}]^{-0.5} \end{aligned} \tag{3.24}$$

where $A = q^\alpha q_\alpha$, $B = p^\alpha p_\alpha$, and $C = p^\alpha q_\alpha$.

Using (3.23) and (3.24) the trapped surface equation can be expressed as,

$$[Ap^\alpha{}_{|\beta} p^\beta + Bq^\alpha{}_{|\beta} q^\beta - 2Cp^\alpha{}_{|\beta} q^\beta] s_\alpha = (AB - C^2)(K_{\alpha\beta} s^\alpha s^\beta - trK)$$

Expansion of the covariant derivatives yields,

$$\begin{aligned} &[A(\frac{\partial^2 x^\alpha}{\partial \epsilon^2} + \Gamma^\alpha_{\beta\kappa} \frac{\partial x^\beta}{\partial \epsilon} \frac{\partial x^\kappa}{\partial \epsilon}) + B(\frac{\partial^2 x^\alpha}{\partial \mu^2} + \Gamma^\alpha_{\beta\kappa} \frac{\partial x^\beta}{\partial \mu} \frac{\partial x^\kappa}{\partial \mu}) \\ &- 2C(\frac{\partial^2 x^\alpha}{\partial \epsilon \partial \mu} + \Gamma^\alpha_{\beta\kappa} \frac{\partial x^\beta}{\partial \epsilon} \frac{\partial x^\kappa}{\partial \mu})] s_\alpha = (AB - C^2)(K_{\alpha\beta} s^\alpha s^\beta - trK) \end{aligned} \tag{3.25}$$

where $\Gamma^\alpha_{\beta\kappa}$ are the connection coefficients with respect to $\gamma_{\alpha\beta}$.

The vector s_α can be computed from the orthogonality of the space-like basis as,

$$s_\alpha = \frac{\sqrt{\gamma}}{\sqrt{AB - C^2}} \epsilon_{\alpha\beta\kappa} \frac{\partial x^\beta}{\partial \epsilon} \frac{\partial x^\kappa}{\partial \mu} \tag{3.26}$$

where $\gamma = \det\gamma_{\alpha\beta}$ and $\epsilon_{\alpha\beta\kappa}$ is the permutation index. The coefficients A,B and C can be computed as,

$$\begin{aligned} A &= \gamma_{\alpha\beta} \frac{\partial x^\alpha}{\partial \mu} \frac{\partial x^\beta}{\partial \mu} \\ B &= \gamma_{\alpha\beta} \frac{\partial x^\alpha}{\partial \epsilon} \frac{\partial x^\beta}{\partial \epsilon} \\ C &= \gamma_{\alpha\beta} \frac{\partial x^\alpha}{\partial \epsilon} \frac{\partial x^\beta}{\partial \mu} \end{aligned} \tag{3.27}$$

An attempt can be made to solve (3.25) on $\Sigma(\tau)$ once the initial data $(\gamma_{\alpha\beta}, K_{\alpha\beta})$ on $\Sigma(\tau)$ have been specified.

3.4 Methods of Solving the Trapped Surface Equation

In this section a review will be given of various methods that have been used to solve the trapped surface equation. The advantages and disadvantages of each method will be discussed more fully in chapter 4.

3.4a The Trapped Surface Equation in Circular Cylindrical Coordinates

3.4a(i) Axially Symmetric Initial Data

In the case of axially symmetric initial data, each marginally outer trapped surface is most easily expressed in cylindrical coordinates (ρ, z, ϕ) as,

$$\rho = \rho(\epsilon), \quad z = z(\epsilon), \quad \phi = \phi$$

where the surface is parametrised by ϵ, and the z-axis is chosen along the axis of symmetry. The trapped surface equation (3.25) in these coordinates takes the form,

$$[A(\frac{\partial^2 x^{\bar{\alpha}}}{\partial \epsilon^2} + \Gamma^{\bar{\alpha}}_{\bar{\beta}\bar{\kappa}} \frac{\partial x^{\bar{\beta}}}{\partial \epsilon} \frac{\partial x^{\bar{\kappa}}}{\partial \epsilon}) + B\Gamma^{\bar{\alpha}}_{\phi\phi} - 2C\Gamma^{\bar{\alpha}}_{\bar{\beta}\rho} \frac{\partial x^{\bar{\beta}}}{\partial \epsilon}] s_{\bar{\alpha}} = (AB - C^2)(K_{\alpha\beta} s^\alpha s^\beta - trK) \tag{3.28}$$

where barred Greek indices cover the range 1,2. No summation is implied over the indices ρ, ϕ.

For time-symmetric initial data ($K_{\alpha\beta} = 0$) that are conformally flat, $\gamma_{\alpha\beta} = \psi^4 \eta_{\alpha\beta}$ ($\eta_{\alpha\beta} \equiv$ Minkowski three-metric), equation (3.28) reduces to,

$$\frac{1}{\psi^2(\dot{\rho}^2 + \dot{z}^2)}(\dot{z}\ddot{\rho} - \dot{\rho}\ddot{z}) + \frac{4}{\psi^3}(\dot{\rho}\psi_{,z} - \dot{z}\psi_{,\rho}) - \frac{\dot{z}}{\rho\psi^2} = 0 \tag{3.29}$$

where a dot denotes differentiation with respect to ϵ. In this case each marginally outer trapped surface is a minimal surface and Cadez (1974) derived equation (3.29) from this requirement. If a suitable gauge is chosen for ϵ the trapped surface equation reduces to a system of two second order ordinary differential equations. The gauge condition can be formulated as,

$$\dot{\rho}^2 + \dot{z}^2 = W^2 \tag{3.30}$$

where W is the gauge function. Equation (3.29) then reduces to:

$$\begin{aligned} \ddot{z} - WW_{,z} - \frac{\dot{z}\dot{\rho}}{W^2}[WW_{,\rho} - \frac{4W^2}{\psi}\psi_{,\rho} - \frac{W^2}{\rho}] + \frac{\dot{\rho}^2}{W^2}[WW_{,z} - \frac{4W^2}{\psi}\psi_{,z}] = 0 \\ \ddot{\rho} - WW_{,\rho} - \frac{\dot{z}^2}{W^2}[WW_{,\rho} - \frac{4W^2}{\psi}\psi_{,\rho} - \frac{W^2}{\rho}] + \frac{\dot{z}\dot{\rho}}{W^2}[WW_{,z} - \frac{4W^2}{\psi}\psi_{,z}] = 0 \end{aligned} \tag{3.31}$$

The axial symmetry imposes the boundary condition,

$$\dot{z} = 0 \text{ at } \rho = 0 \tag{3.32}$$

Equation (3.31) can be integrated numerically once a gauge function , W, has been chosen. The starting point of the integration is at $z = z_0$, $\rho = 0$, $\epsilon = 0$ and the conditions (3.30) and (3.32) are used as initial constraints. If the path of integration returns to the z-axis with $\dot{z} = 0$ then it is closed and is a marginally outer trapped surface. Any paths of integration that tend to infinity or end on a singularity are ignored. By varying the starting point, z_0, of the integration on the z-axis, the marginally outer trapped surfaces and the apparent horizon can be determined.

Cadez (1974) and Bishop (1982,1984) used this method to treat the axially symmetric case of two Schwarzschild black holes on a surface of time-symmetry using the conformally flat initial data of Misner and Wheeler (1957). Cadez (1974) made the gauge choice $W = \psi^4$ while the results of Bishop (1982) can be reproduced using a gauge $W = \frac{1}{\rho\psi^4}$. Bishop (1984) also used this method to investigate the case of two Schwarzschild black holes where one black hole has very low mass. Slightly different coordinates were used in this case to avoid numerical difficulties.

3.4b The Trapped Surface Equation in Spherical Polar Coordinates

As discussed in chapter 1, the full (3+1) formulation of numerical relativity has been increasingly used to model complex systems of astrophysical interest, which may soon include such systems as two colliding Kerr black holes. This has provided a strong motivation to develop numerical techniques for the solution of the trapped surface equation (3.25) where there are no special symmetries in the initial data. This problem was first addressed by Nakamura, Kojima and Oohara (1984).

In the general case the S^2 topology of the marginally outer trapped surfaces suggests the use of spherical polar coordinates (r, θ, ϕ). The marginally outer trapped surfaces can be defined in these coordinates as $r = r(\theta, \phi)$, where the identification

$\epsilon \equiv \theta, \quad \mu \equiv \phi$ has been made in (3.22) (Nakamura, Kojima and Oohara 1984). The space-like normal to the two-surface, s_α, has components (3.26),

$$s_\alpha = \frac{\sqrt{\gamma}}{\sqrt{AB - C^2}}(1, -\frac{\partial r}{\partial \theta}, -\frac{\partial r}{\partial \phi}) \tag{3.33}$$

The trapped surface equation in these coordinates takes the form,

$$\begin{aligned}
&\frac{\partial^2 r}{\partial \theta^2} + \frac{B}{A}\frac{\partial^2 r}{\partial \phi^2} - \frac{2C}{A}\frac{\partial^2 r}{\partial \theta \partial \phi} \\
&- \frac{\partial r}{\partial \theta}(-2\Gamma^r_{r\theta} + \Gamma^\theta_{\theta\theta} + \frac{B}{A}\Gamma^\theta_{\phi\phi} + \frac{2C}{A}\Gamma^r_{r\phi} - \frac{2C}{A}\Gamma^\theta_{\theta\phi}) \\
&- \frac{\partial r}{\partial \phi}(\Gamma^\phi_{\theta\theta} - \frac{2B}{A}\Gamma^r_{r\phi} + \frac{B}{A}\Gamma^\phi_{\phi\phi} + \frac{2C}{A}\Gamma^r_{r\theta} - \frac{2C}{A}\Gamma^\phi_{\theta\phi}) \\
&- (\frac{\partial r}{\partial \theta})^2(-\Gamma^r_{rr} + 2\Gamma^\theta_{r\theta} - \frac{2C}{A}\Gamma^\theta_{r\phi}) - (\frac{\partial r}{\partial \phi})^2(-\frac{B}{A}\Gamma^r_{rr} + \frac{2B}{A}\Gamma^\phi_{r\phi} - \frac{2C}{A}\Gamma^\phi_{r\theta}) \\
&- (\frac{\partial r}{\partial \theta})^3\Gamma^\theta_{rr} - \frac{B}{A}(\frac{\partial r}{\partial \phi})^3\Gamma^\phi_{rr} \\
&- \frac{\partial r}{\partial \theta}\frac{\partial r}{\partial \phi}(2\Gamma^\phi_{r\theta} + \frac{2B}{A}\Gamma^\theta_{r\phi} + \frac{2C}{A}\Gamma^r_{rr} - \frac{2C}{A}\Gamma^\theta_{r\theta} - \frac{2C}{A}\Gamma^\phi_{r\phi}) \\
&- (\frac{\partial r}{\partial \theta})^2(\frac{\partial r}{\partial \phi})(\Gamma^\phi_{rr} - \frac{2C}{A}\Gamma^\theta_{rr}) - (\frac{\partial r}{\partial \phi})^2(\frac{\partial r}{\partial \theta})(\frac{B}{A}\Gamma^\theta_{rr} - \frac{2C}{A}\Gamma^\phi_{rr}) \\
&+ \Gamma^r_{\theta\theta} + \frac{B}{A}\Gamma^r_{\phi\phi} - \frac{2C}{A}\Gamma^r_{\theta\phi} = \frac{(AB - C^2)^{\frac{1}{2}}}{\sqrt{\gamma}}(K_{\alpha\beta}s^\alpha s^\beta - \mathrm{tr}K)
\end{aligned} \tag{3.34}$$

No summation is implied over the indices r, θ, ϕ.

Specializing to the case of conformally flat initial data, $\gamma_{\alpha\beta} = \psi^4 \eta_{\alpha\beta}$ ($\eta_{\alpha\beta} \equiv$ Minkowski three-metric), equation (3.34) becomes,

$$
\begin{aligned}
&\frac{\partial^2 r}{\partial\theta^2} + \frac{B}{A}\frac{\partial^2 r}{\partial\phi^2} - \frac{2C}{A}\frac{\partial^2 r}{\partial\theta\partial\phi} \\
&\quad + \frac{\partial r}{\partial\theta}\left(\frac{B}{A}\sin^2\theta\left(\frac{\psi_{,\theta}}{2\psi} + \cot\theta\right) + \frac{\psi_{,\theta}}{2\psi}\right) \\
&\quad + \frac{\partial r}{\partial\phi}\left(\frac{\psi_{,\phi}}{2\psi\sin^2\theta}\left(1 + \frac{B}{A}\sin^2\theta\right) + \frac{2C}{A}\cot\theta\right) \\
&\quad + \frac{\partial r}{\partial\theta}\frac{\partial r}{\partial\phi}\left(\frac{2C}{A}\left(\frac{\psi_{,r}}{2\psi} + \frac{2}{r}\right)\right) - \frac{\partial r}{\partial\theta}\left(\frac{\partial r}{\partial\phi}\right)^2\left(-\frac{B}{2Ar^2\psi}\psi_{,\theta} + \frac{C}{A}\frac{\psi_{,\phi}}{r^2\psi\sin^2\theta}\right) \qquad (3.35) \\
&\quad - \left(\frac{\partial r}{\partial\theta}\right)^2\frac{\partial r}{\partial\phi}\left(\frac{C}{Ar^2\psi}\psi_{,\theta} - \frac{1}{2r^2\psi\sin^2\theta}\psi_{,\phi}\right) + \left(\frac{\partial r}{\partial\phi}\right)^3\left(\frac{B}{2Ar^2\psi\sin^2\theta}\psi_{,\phi}\right) \\
&\quad + \left(\frac{\partial r}{\partial\theta}\right)^3\left(\frac{1}{2r^2\psi}\psi_{,\theta}\right) - \left(\frac{\partial r}{\partial\phi}\right)^2\left(\frac{B}{A}\left(\frac{\psi_{,r}}{2\psi} + \frac{2}{r}\right)\right) - \left(\frac{\partial r}{\partial\theta}\right)^2\left(\frac{\psi_{,r}}{2\psi} + \frac{2}{r}\right) \\
&\quad - \frac{r}{2\psi}(r\psi_{,r} + 2\psi)\left(1 + \frac{B}{A}\sin^2\theta\right) = \frac{(AB - C^2)^{\frac{1}{2}}}{\sqrt{\gamma}}(K_{\alpha\beta}s^\alpha s^\beta - trK)
\end{aligned}
$$

The coefficients A,B and C can be calculated from (3.27) as,

$$A = \psi^4\left(\frac{\partial r}{\partial\phi}\right)^2 + \psi^4 r^2\sin^2\theta$$

$$B = \psi^4\left(\frac{\partial r}{\partial\theta}\right)^2 + \psi^4 r^2$$

$$C = \psi^4\left(\frac{\partial r}{\partial\theta}\right)\left(\frac{\partial r}{\partial\phi}\right)$$

The space-like normal to the two-surface, s_α, can be calculated from (3.33) while the extrinsic curvature $K_{\alpha\beta}$ depends on $\Sigma(\tau)$, the hypersurface slicing of the space-time.

Equation (3.35) is a highly non-linear second-order partial differential equation of mixed type. All attempts to solve this equation have used series methods and these will be discussed in the next two sections.

3.4b(i) Axially Symmetric Initial Data

In the case of axial symmetry, where the z-axis is chosen to lie along the axis of symmetry, all terms in equations (3.34) and (3.35) involving $\frac{\partial r}{\partial \phi}$ vanish. The marginally outer trapped surfaces, $r(\theta)$, can be approximated as a truncated series expansion of the form,

$$r(\theta) = \sum_{l=0}^{l_{max}} a_l P_l(\cos\theta)$$

where $P_l(\cos\theta)$ are the Legendre polynomials.

In the case of time-symmetric initial data, the marginally outer trapped surfaces coincide with minimal surfaces (Gibbons 1972) and the coefficients, a_l, can be determined from a variational principle. For conformally flat initial data, $\gamma_{\alpha\beta} = \psi^4 \eta_{\alpha\beta}$, the area of a surface $r = r(\theta, \phi)$ is given by,

$$A_s = \int_0^{2\pi} \int_0^{\pi} \psi^4 [r^2 \sin^2\theta + \sin^2\theta (\frac{\partial r}{\partial \theta})^2 + (\frac{\partial r}{\partial \phi})^2]^{\frac{1}{2}} r d\theta d\phi \qquad (3.36)$$

The coefficients can be determined numerically from the condition that the two-surface is extremal,

$$\delta A_s = 0 \qquad (3.37)$$

This technique was used by Brill and Lindquist (1963) in determining the apparent horizons for two time-symmetric Reissner-Nordstrom black holes, using the initial data of Misner and Wheeler (1957) generalised to include electric charge.

Eardley (1977) used a similar approach in locating the apparent horizons of axially symmetric pure gravitational radiation. These initial data are also time-symmetric and conformally flat. In this case the marginally outer trapped surfaces were

approximated as,

$$r(\theta) = \sum_{l=0}^{l_{max}} a_l \cos^l \theta \tag{3.38}$$

Using this expansion, the trapped surface equation (3.35) can be written as,

$$R_{res}(a_l, \theta) = 0, \text{ for all } \theta \text{ and } l = 0, .., l_{max} \tag{3.39}$$

where R_{res} is the equation residual obtained by substituting (3.38) in the trapped surface equation. The series coefficients a_l were varied independently to minimise $\int_0^\pi R_{res} d\theta$. This is an iterative technique and requires an initial set of coefficients, $a_l{}^{(0)}$.

3.4b(ii) General Initial Data

For the case of general non-axisymmetric initial data, Nakamura, Kojima and Oohara (1984) approximated the marginally outer trapped surfaces as,

$$r(\theta, \phi) = \sum_{l=0}^{l_{max}} \sum_{m=-l}^{l} a_{lm} Y_{lm}(\theta, \phi) \tag{3.40}$$

where $Y_{lm}(\theta, \phi)$ are the spherical harmonic functions and both a_{lm} and Y_{lm} are complex.

For time-symmetric initial data the coefficients a_{lm} could be determined using the method of Brill and Lindquist (1963), as discussed in the previous section (3.37). The method used by Eardley (1977) could also be generalised to the full (3+1) formulation of numerical relativity by writing the trapped surface equation as,

$$R_{res}(a_{lm}, \theta, \phi) = 0, \text{ for all } \theta, \phi \text{ and } l = 0, .., l_{max}, \quad m = -l, .., l. \tag{3.41}$$

where R_{res} is the equation residual obtained by substituting (3.40) in the trapped surface equation. The coefficients a_{lm} could then be determined by minimising $\int_0^{2\pi} \int_0^{\pi} R_{res} \sin\theta d\theta d\phi$.

Nakamura, Kojima and Oohara (1984), however, proposed a direct iterative scheme for determining the coefficients a_{lm}. This is described in the next section.

3.5 Nakamura's Method

Nakamura's method is based on the series expansion (3.40) for the marginally outer trapped surfaces. The trapped surface equation in spherical polar coordinates (3.34) can be written in the form,

$$\frac{\partial^2 r}{\partial\theta^2} + \cot\theta \frac{\partial r}{\partial\theta} + \frac{1}{\sin^2\theta}\frac{\partial^2 r}{\partial\phi^2} = F(\frac{\partial^2 r}{\partial\theta\partial\phi}, \frac{\partial^2 r}{\partial\phi^2}, \frac{\partial r}{\partial\theta}, \frac{\partial r}{\partial\phi}, \gamma_{\alpha\beta}, K_{\alpha\beta}, \Gamma^{\alpha}_{\beta\kappa}) \qquad (3.42)$$

where the second and third terms on the left hand side have been added to both sides of the equation. This exploits the fact that the spherical harmonic functions Y_{lm} satisfy (Flugge 1974),

$$\frac{\partial^2 Y_{lm}}{\partial\theta^2} + \cot\theta \frac{\partial Y_{lm}}{\partial\theta} + \frac{1}{\sin^2\theta}\frac{\partial^2 Y_{lm}}{\partial\phi^2} = -l(l+1)Y_{lm} \qquad (3.43)$$

Substituting (3.40) in (3.42) and using (3.43) yields,

$$-\sum_{l=0}^{l_{max}} \sum_{m=-l}^{l} l(l+1)a_{lm}Y_{lm} = F(a_{lm}, \gamma_{\alpha\beta}, K_{\alpha\beta}, \Gamma^{\alpha}_{\beta\kappa}) \qquad (3.44)$$

Multiplying both sides of (3.44) by the conjugate spherical harmonic function ${Y_{lm}}^*$ and integrating over all solid angles leads to the relation,

$$a_{lm} = -\frac{1}{l(l+1)} \int_0^{2\pi} \int_0^{\pi} {Y^*}_{lm} F(a_{lm}, \gamma_{\alpha\beta}, K_{\alpha\beta}, \Gamma^{\alpha}_{\beta\kappa}) \sin\theta d\theta d\phi \qquad (3.45)$$

where the orthogonality of the spherical harmonic functions has been exploited (Press et al. 1986),

$$\int_0^{2\pi} \int_0^{\pi} Y_{lm}(\theta,\phi) Y^*{}_{l'm'}(\theta,\phi) \sin\theta d\theta d\phi = \delta^l{}_{l'} \delta^m{}_{m'}$$

The relation (3.45) can be used as the basis for an iterative scheme to determine the coefficients a_{lm}. This can be expressed in algorithmic form as,

begin

(* Calculate an initial set of coefficients $a_{lm}{}^{(0)}$ using a trial solution $r_0(\theta,\phi)$ *)

$$a_{lm}{}^{(0)} = \int_0^{2\pi} \int_0^{\pi} r_0(\theta,\phi) Y^*{}_{lm} \sin\theta d\theta d\phi \qquad (3.46)$$

$$n = 0$$

repeat

$$n = n + 1$$

(* Calculate a new set of coefficients $a_{lm}{}^{(n)}$ using (3.45) for all $1 \leq l \leq l_{max}$, $0 \leq m \leq l$ *)

$$a_{lm}{}^{(n)} = -\frac{1}{l(l+1)} \int_0^{2\pi} \int_0^{\pi} Y^*{}_{lm} F(a_{lm}{}^{(n-1)}, \gamma_{\alpha\beta}, K_{\alpha\beta}, \Gamma^{\alpha}_{\beta\kappa}) \sin\theta d\theta d\phi, \quad (3.47)$$

(* Determine $a_{00}{}^{(n)}$ as the root of the equation *)

$$\int_0^{2\pi} \int_0^{\pi} Y^*{}_{00} F(a_{lm}{}^{(n-1)}, \gamma_{\alpha\beta}, K_{\alpha\beta}, \Gamma^{\alpha}_{\beta\kappa}) \sin\theta d\theta d\phi \; [a_{00}^{(n)}] = 0 \qquad (3.48)$$

until (iteration has converged) or (n exceeds max. no. of iterations allowed);

end

This method was proposed by Nakamura, Kojima and Oohara (1984) as an extension of previous work by Sasaki et al. (1980). The method was demonstrated to work with various trial initial data and was used to treat the case of three time-symmetric Schwarzschild black holes (Oohara, Nakamura and Kojima 1985). This numerical method will be evaluated more fully in the next chapter.

The aim of the evaluation will be to determine the suitability and limitations of the algorithm for general numerical space-times. This will include a more detailed analysis of the accuracy, complexity and convergence of the algorithm than that conducted by Nakamura, Kojima and Oohara (1984). In particular the case of two time-symmetric Schwarzschild black holes will be treated, where a numerical solution has been determined by other means and highly distorted marginally outer trapped surfaces are known to exist (Bishop 1982,1984).

CHAPTER FOUR

NUMERICAL EVALUATION OF THE NAKAMURA ALGORITHM

Introduction

This chapter deals with the numerical evaluation of the Nakamura algorithm. The implementation of the algorithm is described in section 4.1. The first test problem considered is that of a shifted Schwarzschild black hole (section 4.2). The computational complexity of the algorithm is discussed in section 4.3. Several modifications are made to the algorithm and these are given in section 4.4. The second test problem considered is that of two time-symmetric Schwarzschild black holes (section 4.5). In section 4.6 the case of three collinear, time-symmetric Schwarzschild black holes is considered. In closing, the algorithm is compared with other numerical methods in section 4.7.

4.1 Implementation of the Nakamura Algorithm

This section contains a brief description of the implementation of the Nakamura algorithm, and a discussion of the numerical methods that were used.

The algorithm was coded in FORTRAN 77 on an IBM 3083. Use was made of subroutines from the Numerical Algorithms Group (NAG) library (NAG Library Manual 1982) and the IMSL MATH/LIBRARY (IMSL Library Reference 1987).

4.1a The Spherical Harmonic Functions

The spherical harmonic functions, $Y_{lm}(\theta, \phi)$, are defined in terms of the associated

Legendre functions $P^m{}_l(\cos\theta)$ as (Press et al. 1987),

$$Y_{lm}(\theta,\phi) = \sqrt{\frac{(2l+1)}{4\pi}\frac{(l-m)!}{(l+m)!}}P^m{}_l(\cos\theta)e^{im\phi} \tag{4.1}$$

The order, l, and degree, m, of the functions are integers in the range $l \geq 0, \quad -l \leq m \leq l$.

The spherical harmonic functions are orthogonal for different l,m when integrated over a sphere,

$$\int_0^{2\pi}\int_0^{\pi} Y_{lm}(\theta,\phi)Y^*_{l'm'}(\theta,\phi)\sin\theta d\theta d\phi = \delta_{l'l}\delta_{m'm} \tag{4.2}$$

and also satisfy (Press et al. 1987),

$$Y_{l,-m}(\theta,\phi) = (-1)^m Y^*_{lm}(\theta,\phi) \tag{4.3}$$

The associated Legendre polynomials can be expressed in a hypergeometric series representation (Gradshteyn and Ryzhik 1980,p1009) but this is not optimal for numerical work. A more computationally stable and robust method is suggested by Press et al. (1987) based on the reccurrence scheme,

$$(l-m)P^m{}_l = (\cos\theta)(2l-1)P^m{}_{l-1} + (l+m-1)P^m{}_{l-2} \tag{4.4}$$

For the special case of $l = m+1$ this becomes,

$$P^m{}_{m+1} = (\cos\theta)(2m+1)P^m{}_m \tag{4.5}$$

The associated Legendre polynomials $P^m{}_m$ have the closed form expression (Press et al. 1987),

$$P^m{}_m(\cos\theta) = (-1)^m(\sin\theta)^m\prod_{i=1}^{m}(2i-1) \tag{4.6}$$

Equations (4.6) and (4.5) thus provide the two starting values for the reccurrence relation (4.4). The first and second derivatives of the associated Legendre polynomials can be calculated in the same way by differentiating equations (4.4),(4.5) and (4.6). Due to the property (4.3) it is only ever neccessary to evaluate polynomials of positive degree, i.e. $m \geq 0$.

4.1b Evaluation of $r(\theta, \phi)$ and its derivatives

In the Nakamura algorithm the marginally outer trapped surfaces $r(\theta, \phi)$ are approximated as (3.40),

$$r(\theta, \phi) = \sum_{l=0}^{l_{max}} \sum_{m=-l}^{l} a_{lm} Y_{lm}(\theta, \phi) \tag{4.7}$$

Exploiting the orthogonality of the spherical harmonic functions (4.2) yields,

$$a_{lm} = \int_0^{2\pi} \int_0^{\pi} Y^*_{lm}(\theta, \phi) r(\theta, \phi) \sin\theta d\theta d\phi \tag{4.8}$$

Using (4.3) and the fact that $r(\theta, \phi)$ is real leads to the relation,

$$a_{l,-m} = (-1)^m a^*_{lm} \tag{4.9}$$

The expansion (4.7) can thus be written as,

$$r(\theta, \phi) = \sum_{l=0}^{l_{max}} [a_{l0} Y_{l0} + 2 \sum_{m=1}^{l} \Re(a_{lm} Y_{lm})] \tag{4.10}$$

where $\Re$ denotes the real part.

The derivatives of $r(\theta, \phi)$ can be derived directly from (4.10); for example,

$$\frac{\partial^2 r}{\partial \theta^2} = \sum_{l=0}^{l_{max}} [a_{l0} \frac{\partial^2 Y_{l0}}{\partial \theta^2} + 2 \sum_{m=1}^{l} \Re(a_{lm} \frac{\partial^2 Y_{lm}}{\partial \theta^2})]$$

In the case of axial symmetry, all coefficients in (4.10) with $m \neq 0$ vanish.

If the series (4.10) is evaluated directly using the reccurrence relation (4.4) for the associated Legendre polynomials, then the computational complexity in evaluating $r(\theta, \phi)$ is of order $\sim O(l_{max}^3)$. It is more efficient to evaluate $r(\theta, \phi)$ as,

$$r(\theta, \phi) = \sum_{l=0}^{l_{max}} a_{l0} Y_{l0} + 2 \sum_{m=1}^{l_{max}} \sum_{l=m}^{l_{max}} \Re(a_{lm} Y_{lm})$$

This evaluation is optimal for the reccurrence relation and is of computational complexity $\sim O(l_{max}^2)$.

4.1c Other numerical methods used

4.1c(i) Numerical Quadrature

Numerical integration is required in steps (3.46),(3.47) and (3.48) of the Nakamura algorithm. The integrals are complex and have the general form,

$$S = \int_0^{2\pi} \int_0^{\pi} Y_{lm}^* G(\theta, \phi) \sin\theta d\theta d\phi$$

where $G(\theta, \phi)$ is a smooth real function of θ and ϕ. The real and imaginary parts are evaluated separately. Using (4.1) the real part of S can be written as,

$$\Re(S) = \sqrt{\frac{2l+1}{4\pi} \frac{(l-m)!}{(l+m)!}} \int_0^{2\pi} \int_0^{\pi} P_l^m(\cos\theta) G(\theta, \phi) \sin\theta d\theta \cos(m\phi) d\phi$$

The imaginary part is identical except $\cos(m\phi)$ is replaced by $-\sin(m\phi)$. The inner integral over θ is smooth and well-behaved but the outer integral over ϕ is rapidly oscillatory for large m. The intergral S is most easily evaluated by applying a one-dimensional method to each dimension.

A computationally efficient method proved to be the NAG routine D01DAF (NAG Library Reference 1982) which applies a Patterson method to each dimension. The Patterson method is based on optimal extension of the Gauss quadrature formulae (Patterson 1968). The degree of the quadrature formula in use is steadily increased from a three-point Gaussian formula to a 255-point quadrature formula until two successive integral evaluations differ by less than a specified absolute accuracy. This method does not evaluate the integrand on the boundary. This avoids coding difficulties at $\theta = 0, \pi$ due to terms of the form $\frac{1}{\sin\theta}$ in F (3.35).

The results of this method were confirmed by using a combination of two univariate IMSL quadrature routines. The inner integral was evaluated using DQDAGS and the outer integral using DQDAWO (IMSL Library Reference 1987). The routine DQDAGS uses a globally adaptive scheme where a 21-point Gauss-Konrad formula is applied to each subinterval. Extrapolation is also used (Piessens et al. 1983). DQDAWO uses a similar adaptive strategy but allows a $\sin(\omega x)$ or $\cos(\omega x)$ weighting. A modified Curtis-Clenshaw procedure or 7/15 Gauss-Konrod rule is used in each subinterval (Piessens et al. 1983) with extrapolation.

No significant difference was found between the two approaches for $m \leq 10$. The trigonometric weighting is, however, important for larger m. This is consistent with the analysis of rapidly oscillatory Fourier integrals by Davis and Rabinowitz (1975, p125). The NAG routine D01DAF was used for $m \leq 10$ for reasons of computational efficiency. Trigonometric weighting should not be used in evaluating (3.48).

If the marginally outer trapped surfaces $r(\theta, \phi)$ are well-behaved functions, including $r(\theta, \phi) > 0$ for all θ, ϕ, then the integrand F is smooth and well-defined even on the boundary. If $r(\theta, \phi)$ passes through a singular point in the three-surface, where the curvature scalar or conformal factor is infinite, then the integrals (3.47)

and (3.48) are undefined.

4.1c(ii) Roots

The Nakamura algorithm also requires finding a root of the equation (3.48). This is a transcendental equation in a single variable $\Re(a_{00})$.

An initial range for the root is determined by sampling the function at equal spacing in a_{00} and determining all zero crossings. The lower limit for the search is set by the condition $r(\theta,\phi) > 0$ and the upper limit is specified by the user. This can easily be estimated in terms of the scale of the problem. The initial range is passed to the NAG routine C05ADF (NAG Library Manual 1982) which determines the root to within a specified absolute accuraccy using a combination of bisection, linear interpolation and extrapolation.

4.1d Measures of Convergence

The following measures were used to test the convergence of the algorithm:

(i) The integral L_2 norm of the equation residual (3.41),

$$\left[\int_0^{2\pi}\int_0^{\pi} R_{res}^2 \sin\theta d\theta d\phi\right]^{0.5} \tag{4.11}$$

(ii) The integral L_2 norm of the change in the solution $r(a_{lm}^{(n)},\theta,\phi)$ from the previous to the current iteration cycle,

$$\left[\int_0^{2\pi}\int_0^{\pi} (r(a_{lm}^{(n)},\theta,\phi) - r(a_{lm}^{(n-1)},\theta,\phi))^2 \sin\theta d\theta d\phi\right]^{0.5} \tag{4.12}$$

The maximum change in $r(\theta,\phi)$ is also computed as the discrete norm,

$$\|r(a_{lm}^{(n)},\theta,\phi) - r(a_{lm}^{(n-1)},\theta,\phi)\|_{\infty,d}$$

(iii) The change in the area of the surface $r(a_{lm}^{(n)}, \theta, \phi)$ as defined in (3.36).

4.2 Evaluation of the Nakamura Algorithm for a Shifted Schwarzschild Black Hole

In evaluating the Nakamura algorithm it is important to consider the following numerical properties of the method:

(i) Convergence
(ii) Accuracy
(iii) Computational complexity (speed)
(iv) Sensitivity of the algorithm to the initial trial function
(v) Robustness and stability of the algorithm
(vi) Ease of implementation

A useful test of the algorithm can be performed by determining the apparent horizon for a shifted Schwarzschild black hole on a time-symmetric space-like slice. The position of the apparent horizon in this case is known analytically. As there are no special spatial symmetries this is also a test of determining apparent horizons in full (3+1) numerical relativity.

4.2a Initial data for a Shifted Schwarzschild Black Hole

The initial data for a shifted Schwarzschild black hole of mass M in isotropic coordinates on a space-like hypersurface (t=constant) are given in section 2.1b. They are,

$$K_{\alpha\beta} = 0$$

$$\gamma_{\alpha\beta} = (1 + \frac{M}{2R})^4 \eta_{\alpha\beta}, \quad \text{where } \eta_{\alpha\beta} \equiv \text{ Minkowski three-metric}$$

For a black hole centered at $r = d, \theta = \alpha, \phi = \beta$, R is given by,

$$R = [r^2 + d^2 - 2rd(\sin\theta \sin\alpha \cos(\phi - \beta) + \cos\theta \cos\alpha)]^{\frac{1}{2}}$$

In this case the apparent horizon is the shifted three-sphere of radius $\frac{M}{2}$ defined by,

$$r(\theta, \phi) = vd + \sqrt{v^2 d^2 - (d^2 - \frac{M^2}{4})}, \quad d \leq \frac{M}{2} \tag{4.13}$$

where,

$$v = \sin\theta \sin\alpha \cos(\phi - \beta) + \cos\theta \cos\alpha$$

The initial data are conformally flat and time-symmetric, and the trapped surface equation takes the form (3.35).

4.2b Numerical Results

Nakamura, Kojima and Oohara (1984) tested the method for a shifted time- symmetric Schwarzschild black hole of mass $M = 1$ located at $d = 0.2, \alpha = 0.79, \beta = 1.26$. Starting from a trial solution $r_0(\theta, \phi) = 0.5$ they noted that the final numerical results agreed quite well with the analytic solution but provided no detailed analysis of the convergence of the method. A series of length $l_{max} = 20$ was used.

This example was repeated using an initial trial solution $r_0(\theta, \phi) = 5$ which lies in the asymptotically flat region of the initial data surface. This does not assume any prior knowledge of the final solution. The algorithm was found to converge smoothly to a limiting accuracy in the form,

$$\|r(\theta, \phi) - r_{exact}(\theta, \phi)\|_2 \quad \alpha \quad 10^{-\kappa N} \tag{4.14}$$

where $r_{exact}(\theta, \phi)$ is the known analytic solution (4.13) and N is the iteration number. This is shown graphically as the red curve in Fig. 4.1. The rate of convergence, κ, was found to be $\kappa \sim 0.2$.

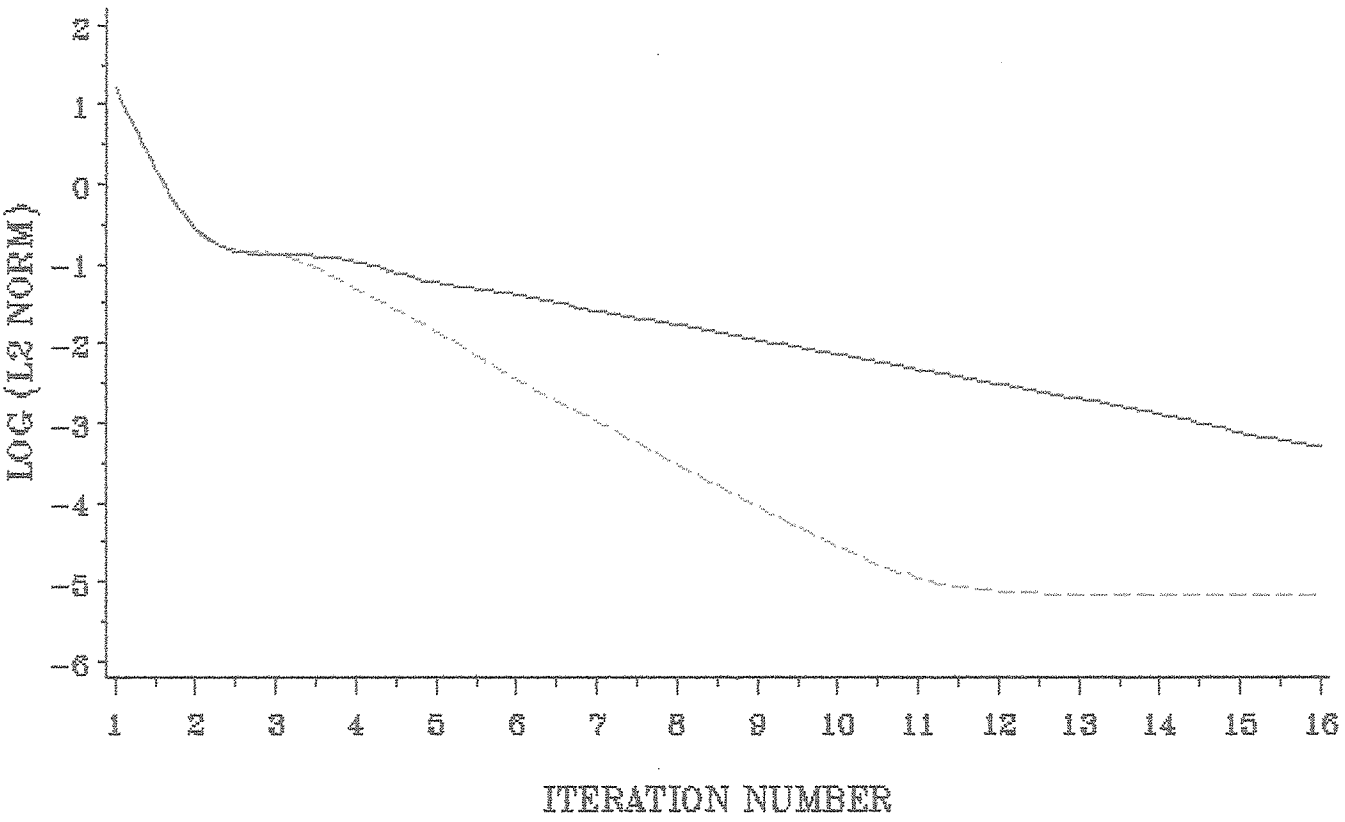

Fig. 4.1 The convergence of the Nakamura algorithm for a shifted Schwarzschild black hole at $d = 0.2, \theta = 0.79, \phi = 1.26$. The convergence, C, is measured as the logarithm of the L_2 norm of the error in the solution i.e.,

$$C = \frac{1}{2}\log\left[\int_0^{2\pi}\int_0^{\pi}[r(\theta,\phi) - r_{exact}(\theta,\phi)]^2 \sin\theta d\theta d\phi\right]$$

The red curve shows the convergence of the original Nakamura algorithm while the green curve depicts the behaviour of the modified Nakamura algorithm.

The limiting accuracy is set by the number of terms in the series and is of order $\sim O(\frac{1}{l_{max}})$. Tests up to $l_{max} \leq 10$ did not indicate a dependence of the rate of convergence κ on l_{max}. Due to computational restrictions $l_{max} = 5$ was used in this example. In addition, the convergence is not strongly influenced by choosing the initial trial solution as either $r_0(\theta, \phi) = 0.5$ or $r_0(\theta, \phi) = 5$.

Now, it is known that for two Schwarzschild black holes on a time-symmetric space-like hypersurface there exist highly distorted marginally outer trapped surfaces (Bishop 1982). Similar surfaces may be expected in the initial data for N black holes which have non-zero linear or angular momentum. It is therefore important to evaluate the Nakamura algorithm for the case of more distorted initial data.

This can be induced as coordinate distortion in the case of a shifted Schwarzschild black hole by increasing the offset, d, of the black hole from the origin. The case $M = 1, d = 0.4, \alpha = 0.79, \beta = 1.26$ was therefore considered. The same initial trial solution $r_0(\theta, \phi) = 5$ was used.

An immediate problem was encountered in determining $a_{00}^{(1)}$ as the equation (3.48) does not have a root for this value of d. This is shown as the green curve in Fig. 4.2. This problem was investigated more fully and is discussed in the next section.

4.2c The Determination of a_{00}

The sensitivity of the Nakamura algorithm to the initial choice of trial solution can be determined analytically for a shifted Schwarzschild black hole.

Consider an initial trial solution $r_0(\theta, \phi) = a = a_{00} Y_{00}$ with origin at $(0, 0, 0)$ for the case of a shifted Schwarzschild black hole of mass M at $r = d, \theta = 0$. The coordinate restriction $d \leq \frac{M}{2}$ is applied.

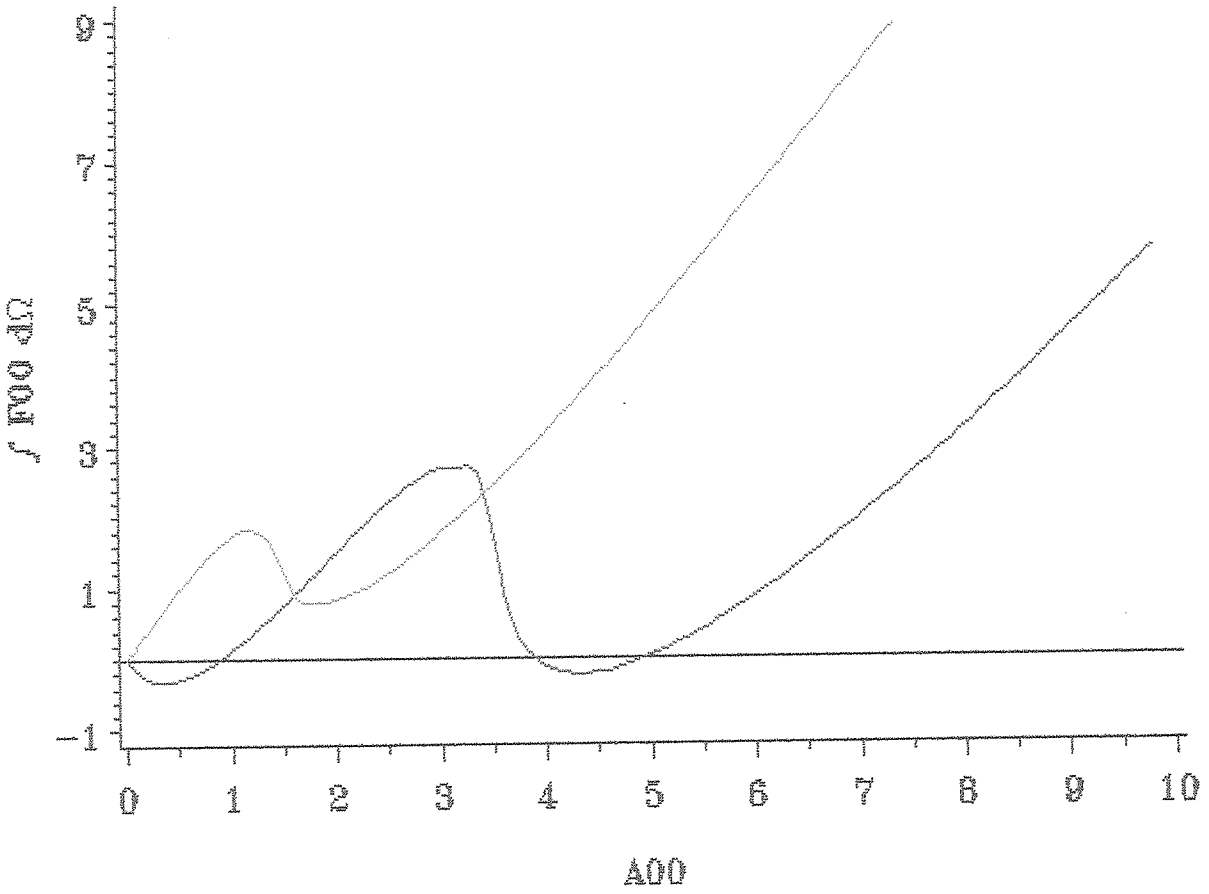

Fig. 4.2 Some examples of the function $\int\int F_{00}\,d\Omega$ (4.19) used in the determination of a_{00}. Both curves depict the function in the first cycle of the iteration with $r_0(\theta,\phi) = 5$ as an initial trial solution. The green curve refers to a shifted Schwarzschild black hole of unit mass situated at $d = 0.4, \theta = 0.79, \phi = 1.26$. In this case a minimum must be accepted for a_{00}. The red curve corresponds to the case of three collinear Schwarzschild black holes of unit mass at equidistant unit spacing, with the origin at the position of the central black hole. The inner root at $a_{00} \sim 1$ results from the marginally outer trapped surface surrounding the central black hole while the root at $a_{00} \sim 5$ is caused by the apparent horizon enclosing all three black holes (cf Fig. 4.9)

Now, a_{00} is determined as the root of the equation $\int_0^{2\pi}\int_0^{\pi} Y_{00}^* F \sin\theta d\theta d\phi = 0$ (3.48). This is essentially a Galerkin criterion (Fletcher 1984).

From (3.35) this becomes,

$$\sqrt{\pi}\int_0^{\pi} \frac{a}{\psi}[a\psi_{,r|r(\theta,\phi)=a} + 2\psi(a,\theta)]\sin\theta d\theta = 0$$

where $\psi = (1+\frac{M}{2R})^4$ and $R = [r^2 + d^2 - 2rd\cos\theta]^{\frac{1}{2}}$.

This can be integrated directly to yield,

$$\begin{aligned} &2\sqrt{\pi}(\frac{d^2-a^2}{d})(\ln(a+d) - \ln|a-d|) + 2\sqrt{\pi}(2a-M) \\ &+ 2\sqrt{\pi}[d(\frac{1}{\eta^2}-1) + \frac{a^2}{d}][\ln(a+d+\frac{M}{2}) - \ln(a-d+\frac{M}{2})] = 0 \end{aligned} \tag{4.15}$$

where η is defined as $d = \eta(\frac{M}{2})$ and $0 < \eta < 1$.

It can be shown numerically that (4.15) has no roots if $\eta \geq 0.46$ although there may be a minimum near the correct value for a_{00}. Thus for a single shifted Schwarzschild black hole of mass $M = 1$ the Nakamura algorithm will not find a root for a_{00} in the first cycle of the iteration if $d \geq 0.23$. The equation (4.15) may have multiple roots and/or minima and needs to be carefully examined in the first few cycles of the iteration. Some representative examples are plotted in Fig. 4.2. In the case of multiple roots the outermost root is usually the best choice but all should be tried for completeness.

The algorithm can be made immediately more robust by accepting minima in (4.15) when there is no root defining a_{00}. This is a Raleigh-Ritz criterion (Fletcher 1984) and is similar to the variational technique used by Brill and Lindquist (1963). In this implementation of the algorithm, minima were determined using the NAG

routine E04JAF which uses a quasi-Newton method with fixed upper and lower bounds on the independent variable. Only function values are used (NAG Library Reference 1982).

The determination of a_{00} can be further improved by constraining $a_{00}^{(n)}$ such that $r(a_{lm}^{(n)}, \theta, \phi)$ is strictly positive. This places a lower limit on the range in which the search is conducted for a root or minimum in (4.15). The original Nakamura method determines the coefficients $a_{lm}^{(n)}$, $l, m \neq 0$ using the relation (3.47) and then determines $a_{00}^{(n)}$ using the previous coefficients $a_{lm}^{(n-1)}$, $l, m \neq 0$. The algorithm is improved in robustness and convergence if $a_{00}^{(n)}$ is determined using $a_{lm}^{(n)}$, $l, m \neq 0$ from the current iteration cycle. This often yields a root in (4.15) where the use of the previous coefficients only leads to a minimum.

Using this method for the determination of a_{00} it is important to monitor the convergence of the algorithm as expressed by the integral L_2 norm of the equation residual (4.11). If equation (4.15) does not develop a root within the first five cycles and the L_2 norm of the equation residual is not converging, then the initial trial solution may need to be improved.

4.2d Further Numerical Results

This improved version of the algorithm was then used for the test problem of a shifted Schwarzschild black hole of mass *M=1* located at $d = 0.4, \alpha = 0.79, \beta = 1.26$ as considered in section 4.2b. The initial trial solution $r_0(\theta, \phi) = 5$ was used with a series of length $l_{max} = 6$. With the improved method for determining a_{00} the iteration was initially convergent but diverged before reaching the limiting accuracy. This is shown by the red curve in Fig. 4.3. The instability was found to be caused by oscillatory behaviour in the coefficients a_{lm}. Tests up to $l_{max} \leq 7$

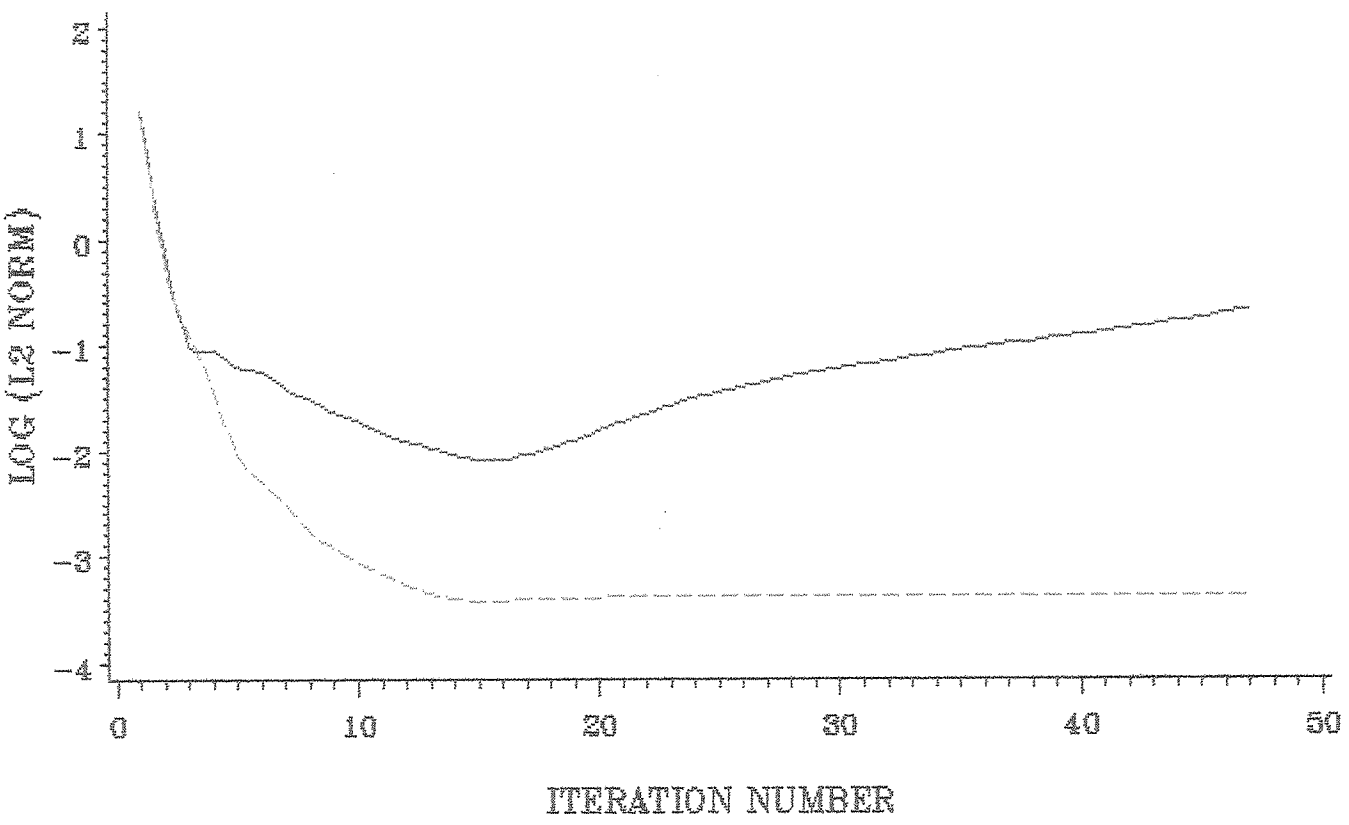

Fig. 4.3 The convergence of the Nakamura algorithm for a shifted Schwarzschild black hole at $d = 0.4, \theta = 0.79, \phi = 1.26$. The convergence, C, is measured as the logarithm of the L_2 norm of the error in the solution i.e.,

$$C = \frac{1}{2}\log\left[\int_0^{2\pi}\int_0^{\pi}[r(\theta,\phi) - r_{exact}(\theta,\phi)]^2 \sin\theta d\theta d\phi\right]$$

The red curve shows the convergence of the original Nakamura algorithm while the green curve depicts the behaviour of the modified Nakamura algorithm.

indicated that this lack of stability is independent of the number of terms in the series approximation for $r(\theta, \phi)$. Tests with greater values of l_{max} proved difficult due to limited computer resources. Divergent behaviour was also found when using an initial trial solution $r_0(\theta, \phi) = 0.5$.

This lack of stability was overcome by taking a weighted average of the coefficients a_{lm} over successive cycles of the iteration. This is analogous to successive overrelaxation as implemented in finite-difference schemes for solving partial differential equations (Quinn 1988,p141). The acceleration is defined in terms of a weighting factor Ω as,

$$a_{lm}^{(n)} = \frac{\Omega a_{lm}^{(n)} + a_{lm}^{(n-1)}}{1 + \Omega} \tag{4.16}$$

It was found that the weighted averaging is best introduced after approximately three iterations. Introducing the weighted average acceleration scheme overcame the previous divergent and unstable behaviour of the algorithm. This is shown by the green curve in Fig. 4.3. In addition, the improved algorithm approximately trebled the convergence rate, κ, for the previous numerical test of the method for a shifted Schwarzschild black hole of mass $M=1$ located at $d = 0.2, \alpha = 0.79, \beta = 1.26$ (as described in section 4.2b). This improvement is shown by the green curve in Fig. 4.1.

The weighted averaging is particularly effective when the coordinate origin is offset from the geometric centre of the marginally outer trapped surface.

4.3 Computational Complexity of the Algorithm

The number of iterations, N_{limit}, needed before convergence to the limiting accuracy is of the order (4.14),

$$N_{limit} \sim O(\frac{1}{\kappa} \log(l_{max}))$$

The computational work, t, per iteration is approximately,

$$t \sim O(l_{max}^4)$$

and the accuracy, ϵ is of order $\sim O(\frac{1}{l_{max}})$. Thus,

$$t \sim O(\frac{1}{\epsilon^4}) \tag{4.17}$$

This is computationally prohibitive but could be reduced by various means.

(i) In a parallel or vectorized computer environment, the coefficients a_{lm} could be iterated in parallel.

(ii) The steps of the algorithm involving numerical quadrature, (3.47) and (3.48), could be considerably optimised by introducing a customized quadrature routine. This would involve sampling the function $F(\theta, \phi)$ at the start of each iteration at a well-defined set of quadrature absisscae over θ and ϕ. This table could be used in determining all the coefficients a_{lm} and would substantially reduce the number of evaluations of the function $F(\theta, \phi)$. This could reduce the computational complexity to the form $t \sim O(\frac{1}{\epsilon^2})$. It would be difficult, however, to introduce trigonometric $\cos(m\phi)$ or $\sin(m\phi)$ weighting over ϕ. This was not investigated further in this research.

(iii) A smaller improvement in speed can be obtained by updating the quadrature accuracy during the course of the iteration. This can be achieved by initially setting the absolute quadrature accuracy ϵ_{lm} for each coefficient a_{lm} to ϵ_0 and updating ϵ_{lm} subject to the constraint,

$$\epsilon_{lm}^{(n+1)} = \frac{[a_{lm}^{(n)} - a_{lm}^{(n-1)}]}{\epsilon_{fact}} \tag{4.18}$$

where ϵ_{fact} is usually 10^2. A lower limit is also set for ϵ_{lm}. This was implemented in the algorithm and led to an increase in computational efficiency.

(iv) The algorithm could also be increased in efficiency by starting with a small number of terms and increasing l_{max} as the iteration converges. This was not investigated further in this research.

4.4 The Modified Nakamura Algorithm

The modified Nakamura algorithm was implemented in the following form:

(* Define variables*)

l_{max}: *highest order in spherical harmonic series for* $r(\theta, \phi)$;
n_{max}: *maximum number of iterations allowed;*
c_{limit}: *convergence limit;*
$r_0(\theta, \phi)$: *initial trial solution;*

(* numerical accuracy parameters *)

ϵ_0: *intial absolute accuracy for quadrature and root finding;*
ϵ_{limit}: *limit to the absolute numerical accuracy;*
ϵ_{fact}: *accuracy adjustment factor;*
ϵ_{lm}: *absolute numerical accuracy used in determining the coefficient* a_{lm}. *This consists of two values for each coefficient, one of the real and one for the imaginary part of each* a_{lm}. *This table is initially set to* ϵ_0.

(* iteration acceleration *)

n_{wait}: *iteration cycle at which to begin averaging the coefficients* a_{lm}
Ω: *weighted average factor;*

begin

(* Determine the initial coefficients $a_{lm}^{(0)}$ using the trial function $r_0(\theta,\phi)$ for all *)

(*$0 \leq l_{max}, \quad 0 \leq m \leq l$. Absolute numerical accuracy: ϵ_0 *)

$$a_{lm}^{(0)} = \int_0^{2\pi} \int_0^{\pi} Y_{lm}^* r_0(\theta,\phi) \sin\theta d\theta d\phi$$

$$n = 0$$

repeat

$$n = n + 1$$

(* Calculate a new set of coefficients $a_{lm}^{(n)}$ using (3.45) for all $1 \leq l \leq l_{max}, \quad 0 \leq m \leq l$. Absolute numerical accuracy: ϵ_{lm}. *)

$$a_{lm}^{(n)} = -\frac{1}{l(l+1)} \int_0^{2\pi} \int_0^{\pi} Y_{lm}^* F(a_{lm}^{(n-1)}, \gamma_{\alpha\beta}, K_{\alpha\beta}, \Gamma^{\alpha}{}_{\beta\kappa}) \sin\theta d\theta d\phi$$

(* Determine $a_{00}^{(n)}$ using the current $a_{lm}^{(n)}$. First determine a lower limit for $a_{00}^{(n)}$ *)

$$a_{00}^{(n)} = 0$$

$$r_{min} = \text{The minimum of } r(a_{lm}^{(n)}, \theta, \phi) \text{ in the interval } \theta = [0,\pi], \quad \phi = [0,2\pi]$$

$$a_{00(min)}^{(n)} = \frac{r_{min}}{Y_{00}}$$

(* Determine $a_{00}^{(n)}$ at the root or minimum of the function *)

$$\int_0^{2\pi} \int_0^{\pi} Y_{00}^* F(a_{lm}^{(n)}, \gamma_{\alpha\beta}, K_{\alpha\beta}, \Gamma_{\alpha\beta}{}^{\alpha}) \sin\theta d\theta d\phi \; [a_{00}^{(n)}] = 0 \qquad (4.19)$$

(* subject to the constraint $a_{00}^{(n)} > a_{00(min)}^{(n)}$. Use the outermost root or mimimum, but try all roots for completeness *)

(* Adjust the numerical accuracy table (4.18) subject to the limit $\epsilon_{lm} \geq \epsilon_{limit}$ *)

for l=0 *to* l_{max} *do*

for m=0 *to* l *do* $\delta a_{lm} = a_{lm}^{(n)} - a_{lm}^{(n-1)}$

if $\delta a_{lm} < \epsilon_{lm}$ *then* $\epsilon_{lm} = \frac{\epsilon_{lm}}{\epsilon_{fact}}$

if $\epsilon_{lm} < \epsilon_{limit}$ *then* $\epsilon_{lm} = \epsilon_{limit}$

(* Compute convergence measures and the area of the surface *)

c_1 : $[\int_0^{2\pi} \int_0^{\pi} R_{res}^2 \sin\theta d\theta d\phi]^{0.5}$

c_2 : $[\int_0^{2\pi} \int_0^{\pi} (r(a_{lm}^{(n)}, \theta, \phi) - r(a_{lm}^{(n-1)}, \theta, \phi))^2 \sin\theta d\theta d\phi]^{0.5}$

c_3 : Area $= A_s = \int_0^{2\pi} \int_0^{\pi} \psi^4 [r^2 \sin^2\theta + \sin^2\theta (\frac{\partial r}{\partial \theta})^2 + (\frac{\partial r}{\partial \phi})^2]^{\frac{1}{2}} r d\theta d\phi$

c_4 : $\|r(a_{lm}^{(n)}, \theta, \phi) - r(a_{lm}^{(n-1)}, \theta, \phi)\|_{\infty,d}$

until $[(c_1 < c_{limit})$ *and* $(c_2 < c_{limit})]$ *or* $(n > n_{max})$;

end;

4.5 Two Time-Symmetric Schwarzschild Black Holes

The second test problem to be considered is the case of two time-symmetric Schwarzschild black holes. This provides a particulalry useful test for the numerical evaluation of the Nakamura algorithm.

Bishop(1982,1984) located a highly distorted marginally outer trapped surface enclosing both black holes, that lies to the interior of the apparent horizon, if the separation between the two black holes is sufficiently small. It is important to determine whether the Nakamura algorithm converges to this solution, particularly as these initial data were not considered by Nakamura, Kojima and Oohara (1984).

The results obtained using the Nakamura algorithm also provide a useful comparison to previous work, which used different numerical methods to determine the apparent horizons of two Schwarzschild black holes. Both the Misner(1963) and the Misner and Wheeler (1957) initial data were considered, and the results are reported in the following sections.

4.5a The Misner and Wheeler Initial Data

The Misner and Wheeler initial data are time-symmetric and conformally flat,

$$K_{\alpha\beta} = 0$$

$$\gamma_{\alpha\beta} = \psi^4 \eta_{\alpha\beta} \quad \text{where } \eta_{\alpha\beta} \equiv \text{ Minkowski three-metric}$$

For two Schwarzschild black holes of mass M_1 and M_2 located at $(r = 0, \theta = 0)$ and $(r = a, \theta = 0)$ respectively, the conformal factor in spherical polar coordinates is given by (2.23),

$$\psi = 1 + \frac{M_1}{2\sqrt{r^2 + d^2 + 2rd\cos\theta}} + \frac{M_2}{2\sqrt{r^2 + (a-d)^2 - 2r(a-d)\cos\theta}}$$

The origin is at $(r = d, \theta = 0)$ and the z-axis is chosen along the line joining the two black holes. In this formulation the initial data are axially symmetric.

4.5a(i) Previous Numerical Results

Apparent horizons for two Schwarzschild black holes, described by the Misner and Wheeler initial data, were originally determined by Brill and Lindquist (1963) using the variational technique of section 3.4b(i). This preliminary work was extended by Cadez (1974) and Bishop(1982,1984) who used the numerical method of section 3.4a(i) to determine the position of the marginally outer trapped surfaces, although both used different gauge choices (3.30). No analytic solution of the trapped surface equation is known for this system.

Bishop(1982) considered the case of two Schwarzschild black holes of unit mass $M_1 = M_2 = 1$ for varying coordinate separation a. For a coordinate separation $a > a_c$, where $a_c \sim 1.53$ there are two components of the apparent horizon, one enclosing each black hole. For large separation a, these components are almost circular with radius $\sim \frac{M}{2}$. As the black holes are brought closer together these component surfaces distort due to gravitational interaction.

For $a \leq a_c$ there are four marginally outer trapped surfaces; one enclosing each black hole and two enclosing both M_1 and M_2. The outermost marginally outer trapped surface is the apparent horizon. This is shown in Fig. 4.4 which is taken from Bishop (1982). In this figure S_3 is the apparent horizon, S_2 is a distorted marginally outer trapped surface enclosing both black holes, and S_{11} and S_{12} are marginally outer trapped surfaces surrounding each individual black hole. The closed trapped region is denoted by cross-hatching. The dotted curves (labelled T_{1-5}) denote paths of integration with $\hat{\theta} = 0$ but which are not closed and hence not marginally outer trapped surfaces. At the critical separation a_c, the surfaces S_2 and S_3 coincide.

The area of the surfaces as a function of separation is shown in Fig. 4.5 (Fig. 2 from Bishop (1982)). Cadez (1974) derived similar results but did not find the surface S_2.

The closed trapped region is defined as the set of points through which there passes a closed trapped surface (section 3.1). Bishop (1982) has shown that as the initial data surface is time-symmetric, surfaces with $\hat{\theta} < 0$ do not extend the closed trapped region. The unhatched region in Fig. 4.4 near $(z = 0.5, \rho = 0)$ is not part of the closed trapped region as there are no closed trapped surfaces such as T_2 passing through this region.

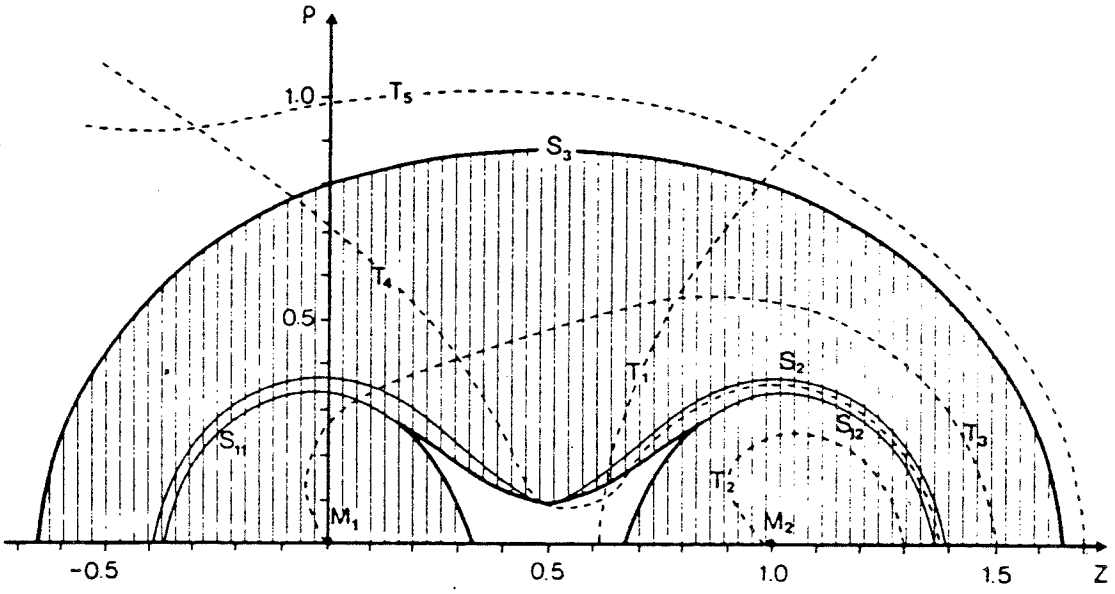

Fig. 4.4 The position of the marginally outer trapped surfaces for two time-symmetric Schwarzschild black holes of unit mass at unit separation. The marginally outer trapped surfaces are denoted by S_{11}, S_{12}, S_2 and S_3. Paths of integration with $\hat{\theta} = 0$ are marked T_{1-5}. The closed trapped region is shaded (taken from Bishop (1982)).

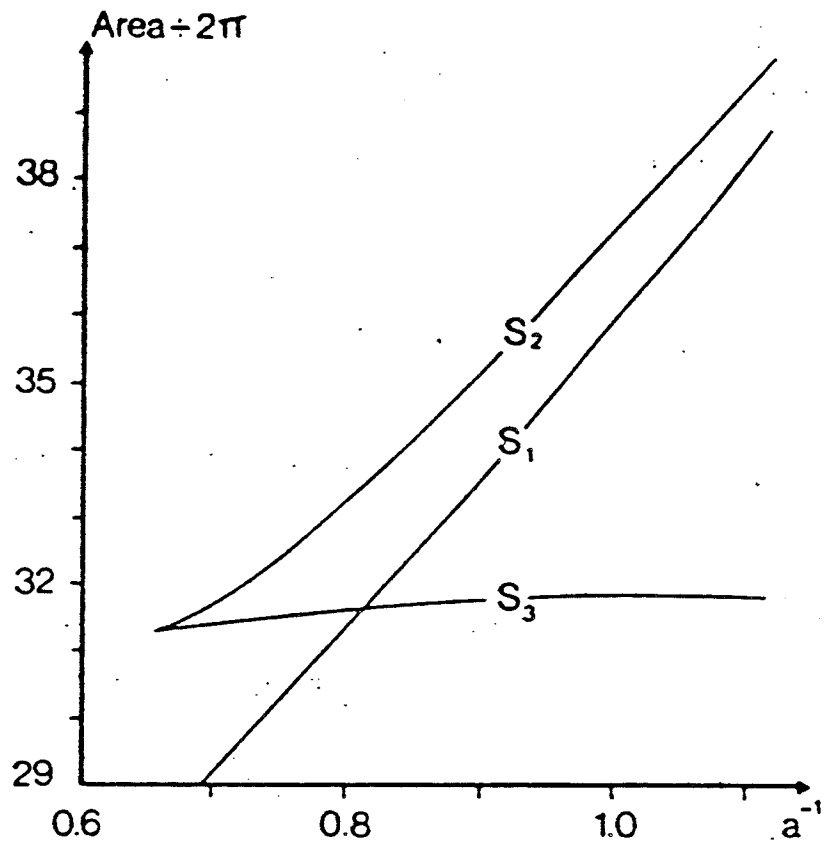

Fig. 4.5 The areas of the marginally outer trapped surfaces $S_1 = (S_{11} + S_{12}), S_2$ and S_3 (Fig. 4.4) shown as a function of (separation)$^{-1}$ (taken from Bishop (1982)).

Bishop (1984) extended this work by considering the case of two Schwarzschild black holes of mass M_1 and M_2 where $M_2 \ll M_1$. The critical separation of the black holes a_c was found to take the asymptotic form (as $M_2 \to 0$),

$$a_c = 0.5M_1 + M_1(0.803 \pm 0.022)(\frac{M_2}{M_1}) \log_e(\frac{M_1}{M_2}) \qquad (4.20)$$

Apparent horizons were determined for a mass ratio $\frac{M_2}{M_1}$ as low as 10^{-6}.

4.5a(ii) Numerical Results using the Nakamura Algorithm

The results of Bishop (1982) for the case $M_1 = M_2 = 1$ were determined using the modified Nakamura algorithm. A series of length $l_{max} = 20$ was used. Due to the axial symmetry only terms with $m = 0$ were computed. Numerical tests using all terms in the series did not yield noticeably different results.

The qualitative behaviour of the marginally outer trapped surfaces as determined by Bishop (1982) was confirmed, with the exception that no surfaces of the type S_2 were found. The position of the marginally outer trapped surfaces for unit separation are shown in Fig. 4.6. Numerous initial trial solutions were used in an attempt to locate surfaces of the form S_2. No success was achieved, even when using the explicit form for S_2 as given in Fig. 1 of Bishop (1982) as the starting point of the iteration. The Nakamura method is not well-suited to determining distorted surfaces of this type.

The critical coordinate separation a_c was found to be consistent with the result $a_c \sim 1.53$ as determined by Cadez (1974). The area of the marginally outer trapped surfaces as a function of coordinate separation is plotted in Fig 4.7. This is consistent with the results of Bishop (1982) as shown in Fig. 4.5.

The algorithm convergence was smooth and stable and took the form (4.14) with

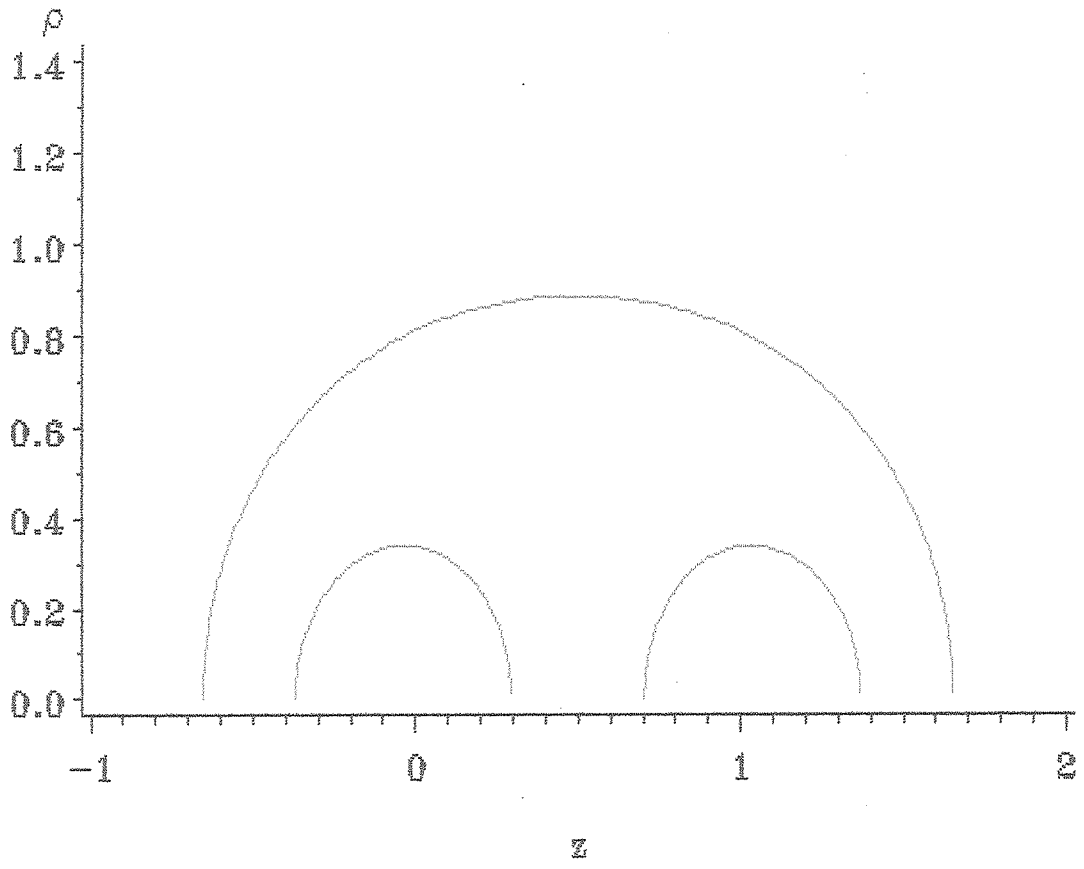

Fig. 4.6 The marginally outer trapped surfaces for two time- symmetric Schwarzschild black holes of mass $M_1 = M_2 = 1$ at unit separation, as determined by the modified Nakamura algorithm. Cylindrical coordinates are used and the black holes are situated at $(z = 0, \rho = 0)$ and $(z = 1, \rho = 0)$.

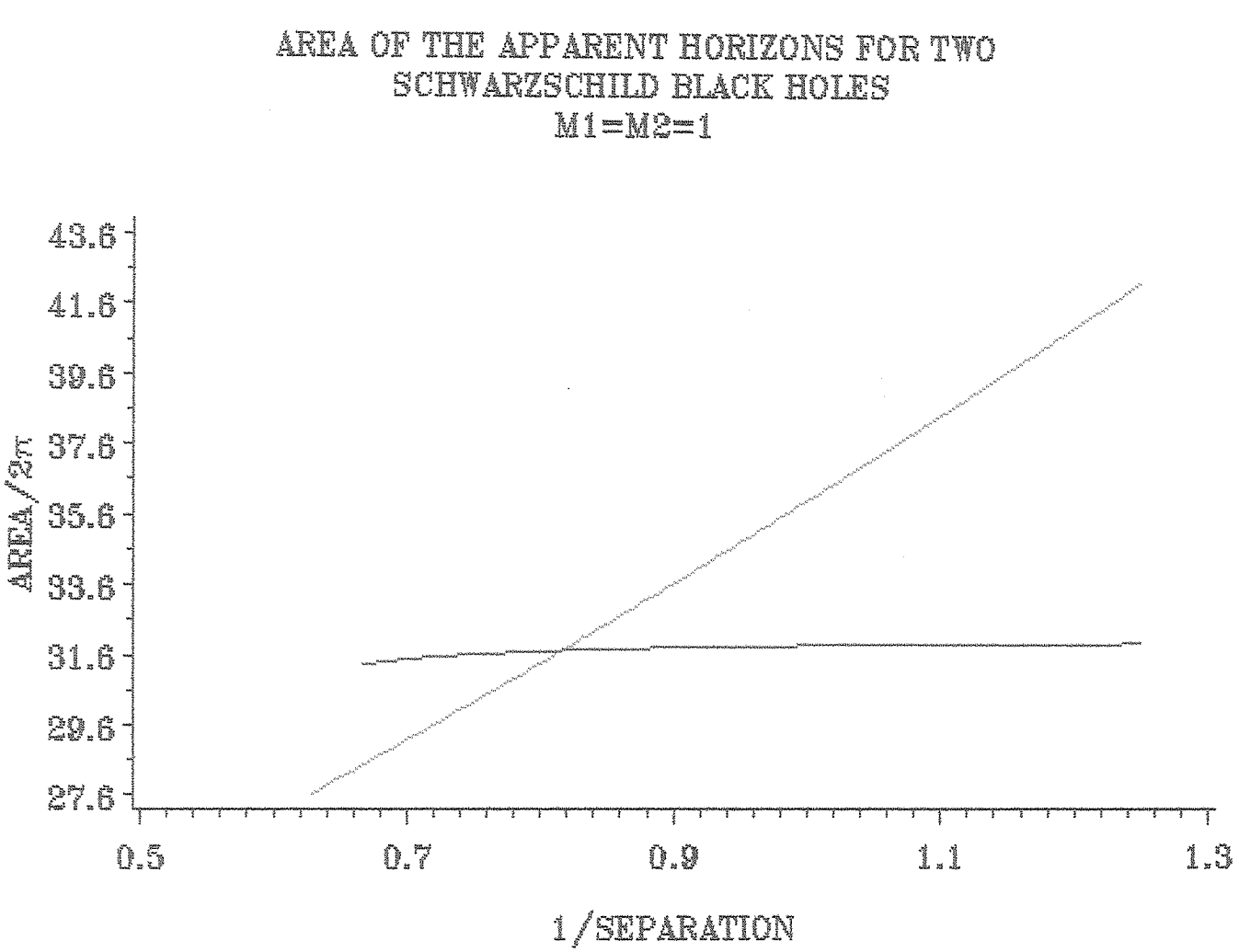

Fig. 4.7 The area of the marginally outer trapped surfaces for two time-symmetric Schwarzschild black holes of unit mass, as determined by the modified Nakamura algorithm. The green curve is the sum of the areas of the inner marginally outer trapped surfaces S_{11} and S_{12} (Fig. 4.4) while the red curve is the area of the outer surface S_3 (Fig 4.4). The red curve has an endpoint at the critical separation $a_c \sim 1.53$.

$\kappa \sim 0.75$. Best results were obtained using a coefficient weighting $\Omega \sim 3$ in (4.16). In determing the apparent horizon S_3 a coordinate origin at $(r = \frac{a}{2}, \theta = 0)$ was used.

The Nakamura algorithm is not well suited to the problem of two black holes with $M_2 \ll M_1$ as considered by Bishop (1984). The positions of the marginally outer trapped surfaces need to be known to high accuracy to reproduce the result (4.20). A large number of terms, l_{max}, are thus required which is computationally demanding. More importantly in this case, at the critical separation, the surfaces S_3 and S_{11} are very closely situated. The Nakamura algorithm, which is iterative, cannot easily be constrained to specifically converge to either S_{11} or S_3. In particular, both surfaces have very similar values for a_{00} (4.19).

4.5b The Misner Initial Data

These initial data were described in section 2.2b and are given by,

$$K_{\alpha\beta} = 0$$

$$\gamma_{\alpha\beta} = \psi^4 \eta_{\alpha\beta}, \text{ where } \eta_{\alpha\beta} \equiv \text{ Minkwoski three-metric}$$

The conformal factor is defined by the relation (2.29) and is inversion symmetric, as discussed in section 2.2b. For the case of two Schwarzschild black holes of equal mass the conformal factor can be written in spherical polar coordinates as (Smarr et al. 1976, Lindquist 1963),

$$\psi = \sqrt{\delta_0}[1 + \sum_{n=1}^{\infty} \text{csch}(n\mu_0)(\frac{1}{+r_n} + \frac{1}{-r_n})]$$

where,

$$\pm r_n = [r^2 + d^2 - 2rd\cos\theta + \coth^2(n\mu_0) \pm (2r\cos\theta\coth(n\mu_0) - 2d\coth(n\mu_0))]^{0.5}$$

The initial data consist of two Einstein-Rosen bridges located at $(r = \delta_0, \theta = 0)$ and $(r = \delta_0, \theta = \pi)$ with the origin at $(r = d, \theta = 0)$. The z-axis is chosen to lie along the axis joining the two throats.

The two free parameters in the initial data, δ_0 and μ_0, are related to the physical characteristics of the system. The total mass of the system, M, as measured at spatial infinity, is defined in terms of these parameters as (Misner 1960),

$$M = 4\delta_0 \sum_{n=1}^{\infty} \operatorname{csch}(n\mu_0) \tag{4.21}$$

Similarly, the proper distance, L, along a space-like geodesic connecting the two throats is given by (Lindquist 1963) as,

$$L = 2\delta_0 [1 + 2\mu_0 \sum_{n=1}^{\infty} n \operatorname{csch}(n\mu_0)]$$

4.5b(i) Previous Numerical Results

The determination of the marginally outer trapped surfaces for two Schwarzschild black holes described by the Misner initial data, was originally considered by Gibbons and Schutz (1972). This preliminary work was extended by Smarr et al. (1976) using the method of Cadez (1974) (section 3.4a(i)). Both papers were primarily concerned with computing the maximum amount of gravitational radiation that could be emitted in the future evolution of the initial data. The maximum efficiency, η, with which the initial rest mass of the system can be converted to gravitational radiation can be defined as (section 3.2),

$$\eta = 1 - \frac{1}{M}\sqrt{\frac{\tilde{A}}{16\pi}} \tag{4.22}$$

where $\tilde{A}$ is the area of the apparent horizon and M is the total rest mass of the system as defined at spatial infinity.

All previous work has considered the case where $\delta_0 = 1$. For a large ratio of proper separation to total mass, $\frac{L}{M}$, the efficiency tends to the Hawking limit ~ 0.29 (Hawking 1972a). As this ratio decreases so does the efficiency. There is a discontinuous drop in the effiency at $\mu_0 = \mu_c \sim 1.362$ (Smarr et al. 1976) which is the point at which an apparent horizon forms which encloses both black holes.

These results were re-determined using the Nakamura algorithm with the intention of both evaluating the algorithm numerically and investigating more closely the efficiency behaviour at $\mu_0 = \mu_c$. It was also hoped to determine whether a surface of the type S_2 (Fig. 4.4) exists for these initial data.

4.5b(ii) Results using the Nakamura Algorithm

The efficiency as a function of μ_0, as determined by the Nakamura algorithm, is shown in Fig. 4.8. This is consistent with the results of Smarr et al. (1976) and confirms the discontinuous behaviour at $\mu_0 = \mu_c$ which initially appeared incomplete. Gibbons and Schutz (1972) postulated that the two efficiency curves should join smoothly but this is shown to be incorrect. This discontinuous behaviour is probably due to the qualitative change in the nature of the initial data at $\mu_0 = \mu_c$. For $\mu_0 > \mu_c$ the initial data represent two dictinct black holes while for $\mu_0 < \mu_c$ the data represent a single, highly distorted black hole.

The qualitative form of the marginally outer trapped surfaces is the same as for the Misner and Wheeler initial data. No surfaces of the type S_2 (Fig. 4.4) were found.

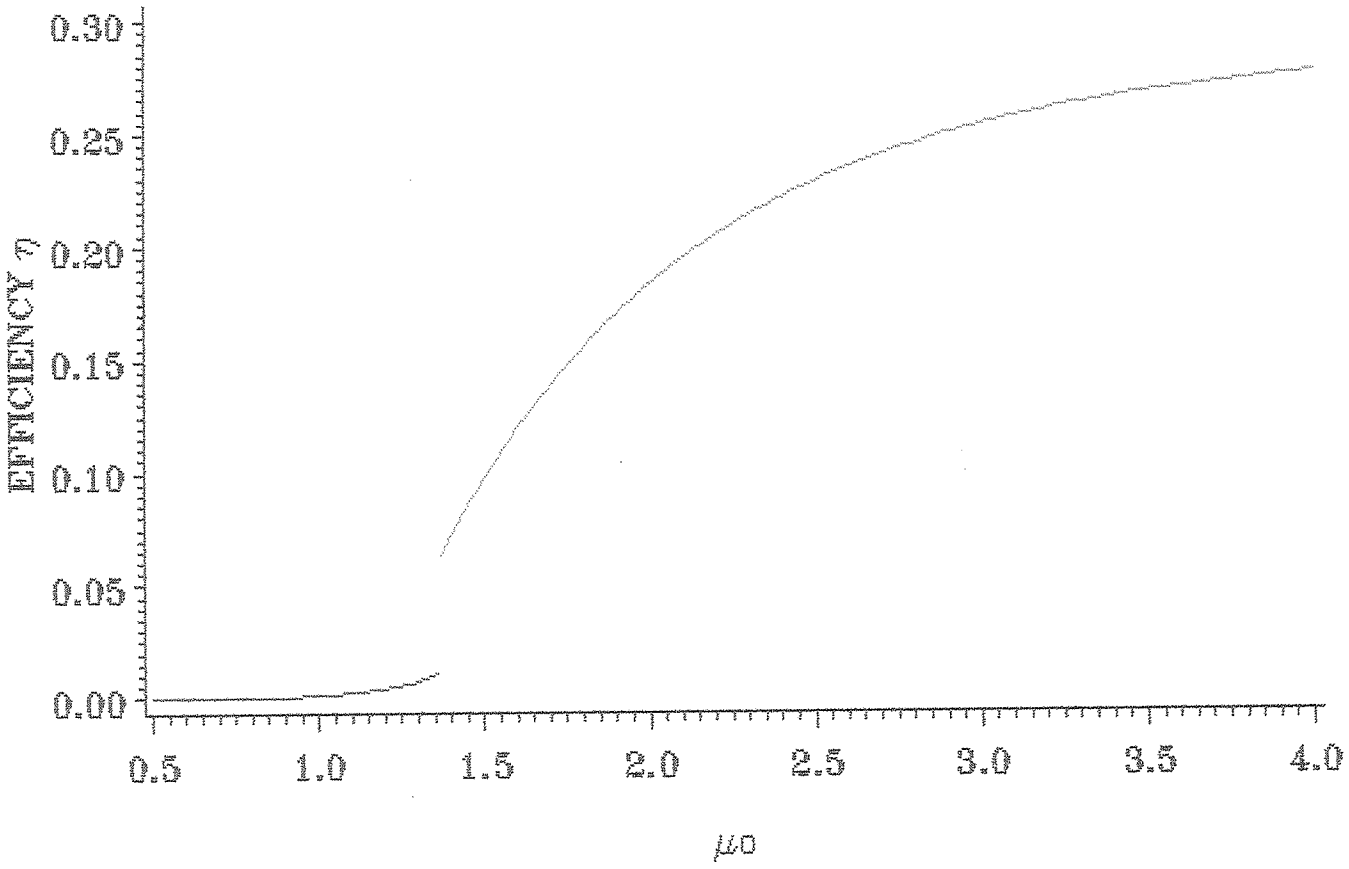

Fig. 4.8 The maximum efficiency for extracting energy from a system of two time-symmetric Schwarschild black holes described by the Misner initial data. The efficiency, η, is plotted as a function of μ_0 (for $\delta_0 = 1$). The ratio of proper distance to mass increases with increasing μ_0. For $\mu_0 \leq 1.36$ there is an apparent horizon enclosing both black holes, and this portion of the graph is shown in red. For $\mu_0 > 1.36$ the efficiency is determined by the area of the apparent horizon components enclosing each individual black hole which is shown by the green curve. There is a discontinuous jump in efficiency at $\mu_0 \sim 1.36$.

4.6 Three Time-Symmetric Schwarzschild Black Holes

In this section apparent horizons are determined for three collinear Schwarzschild black holes on a time-symmetric initial data surface. The black holes are equally spaced and described by the Misner and Wheeler (1957) initial data. An upper bound is obtained for the gravitational radiation expected from the system.

4.6a The Misner and Wheeler Initial Data

The case of three Schwarzschild black holes of mass M_1, M_2 and M_3 at an equidistant spacing, a, along the z-axis, is considered. In spherical polar coordinates the black holes are situated at $(r_j = ja, \theta = 0)$ where j=0,1,2. The initial data are conformally flat and time-symmetric,

$$K_{\alpha\beta} = 0$$

$$\gamma_{\alpha\beta} = \psi^4 \eta_{\alpha\beta}, \text{ where } \eta_{\alpha\beta} \equiv \text{ Minkowski three metric}$$

For a coordinate origin at $(r = d, \theta = 0)$ the conformal factor, ψ, is given by (2.23),

$$\psi = 1 + \sum_{j=0}^{2} \frac{M_j}{2\sqrt{r^2 + (ja - d)^2 - 2r(ja - d)\cos\theta}}$$

The initial data are axially symmetric.

4.6b Numerical Results

Oohara, Nakamura and Kojima (1985) determined the position of the apparent horizon for a system of three Schwarzschild black holes located at the vertices of a regular triangle, with sides of length h. An apparent horizon was found to enclose all three black holes at a critical separation $h_c \sim 2.1$. The maximum efficiency for energy release as defined by equation (4.22) was found to be 8.44 x 10^{-3}.

There are no previous results, however, for the case of three collinear Schwarzschild black holes. This problem was therefore considered using the modified Nakamura algorithm. The black holes were assumed to have unit mass. The qualitative form of the marginally outer trapped surfaces was found to be very similar to the case of two Schwarzschild black holes (section 4.5). A marginally outer trapped surface was found to enclose each black hole. These are slightly distorted from a two-sphere of Schwarzschild radius due to gravitational interaction. At a critical coordinate separation $a_c \sim 1.5$ an apparent horizon forms enclosing all three black holes. The marginally outer trapped surfaces for a coordinate separation $a = 1.45$ are shown in Fig. 4.9.

The maximum efficiency η for the extraction of energy from the system, as defined by equation (4.22), is plotted as a function of coordinate separation in Fig. 4.10. At the critical separation separation $a_c \sim 1.5$ the efficiency η was found to be $\eta \sim 1.2 \text{ x } 10^{-2}$. This is comparable to the result of Oohara, Nakamura and Kojima (1985). The same discontinuous jump in efficiency at the critical separation occurs as in the case of two Schwarzschild black holes (cf Fig.4.8).

4.7 Comparison with Other Numerical Methods

In this section, a comparative survey is given of the various methods for determining apparent horizons in numerical relativity. The general applicability of the Nakamura algorithm is discussed.

As discussed in section 3.4a(i), the method of Cadez (1974) and Bishop (1982) can be used to determine apparent horizons in the case of time-symmetric initial data that are spatially axially symmetric. This method can also be used for initial data that are not time-symmetric and has certain advantages. The primary advantage is that the trapped surface equation, which is in general a second-order non-linear

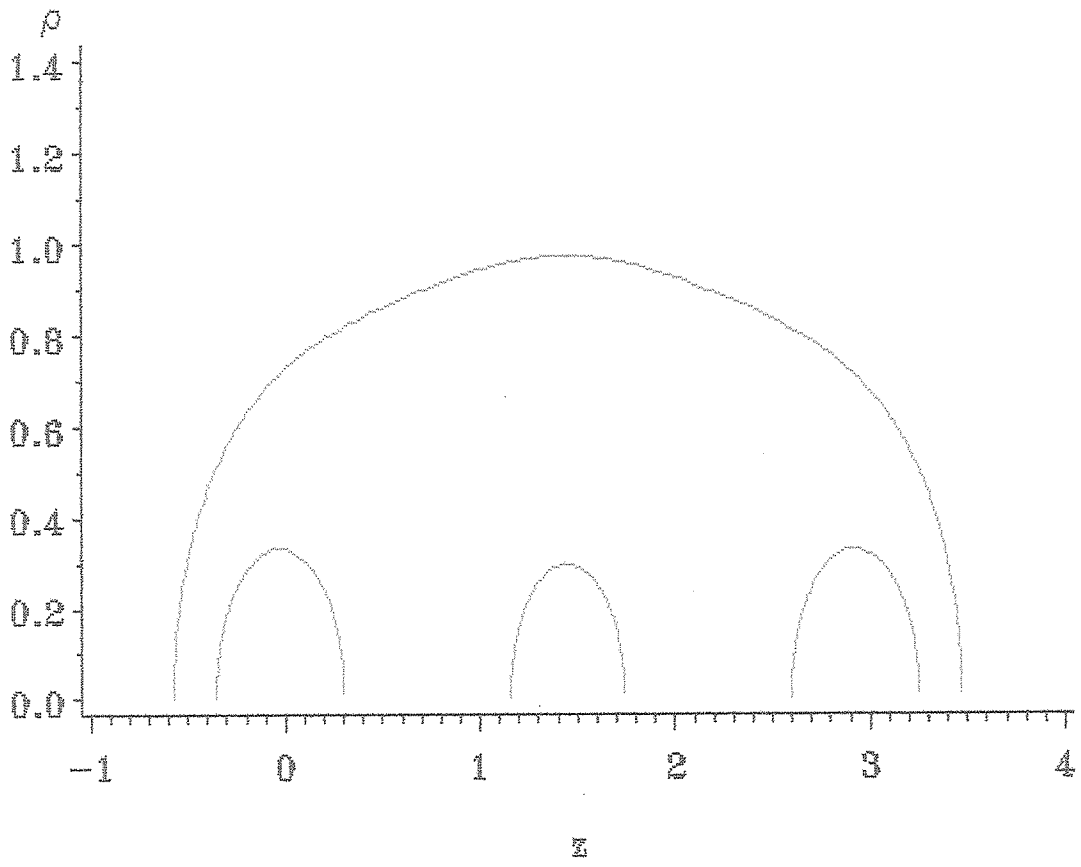

Fig. 4.9 The position of the marginally outer trapped surfaces for three collinear, time-symmetric Schwarzschild black holes of unit mass at an equidistant spacing $a = 1.45$. Cylindrical coorinates are used with the black holes situated at $(z = 0, \rho = 0)$, $(z = 1.45, \rho = 0)$ and $(z = 2.9, \rho = 0)$.

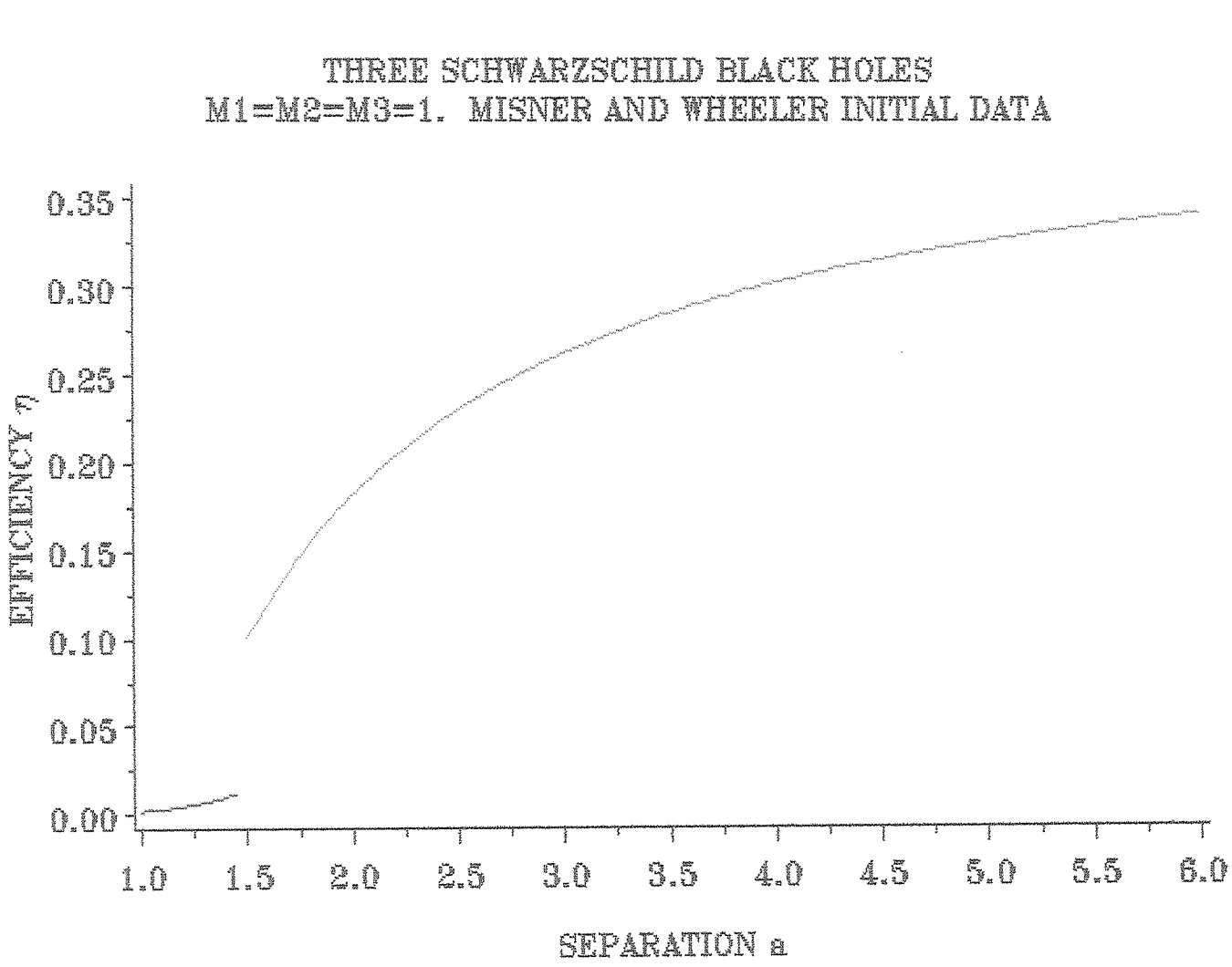

Fig. 4.10 The efficiency for extracting energy from a system of three collinear, time-symmetric Schwarzschild black holes of unit mass. The efficiency ,η, is plotted as a function of the coordinate spacing a between the black holes. The Misner and Wheeler initial data are used. For $a \leq 1.5$ there is an apparent horizon enclosing all three black holes, and this portion of the graph is shown in red. For $a > 1.5$ the efficiency is determined by the area of the apparent horizon components enclosing each individual black hole, and this is shown by the green curve. There is a discontinuous jump in efficiency at the critical separation $a_c \sim 1.5$.

partial differential equation, is reduced to a system of two ordinary differential equations which are easier to solve numerically. This reduces the problem to finding a path in a half-plane. The initial conditions for the numerical integration of the system of ordinary differential equations can be varied to provide fine control over the region in which a search is conducted for a marginally outer trapped surface. This allows a systematic and complete search for all trapped surfaces, and consequently the identification of the closed trapped region. Unfortunately, this method is not easily extended to full (3+1) numerical relativity.

The Nakamura method can also be used for axially-symmetric initial data. In this case only spherical harmonic terms with $m = 0$ are required and the computational complexity is of order $\sim O(\frac{1}{\epsilon^2})$.

For general initial data in full (3+1) numerical relativity, however, the trapped surface equation has to be solved as a non-linear partial differential equation. As discussed in section 3.4b(ii), series methods have been suggested by Eardley (1977) and Nakamura, Kojima and Oohara (1984). The Eardley method is based on the minimisation of the integral L_1 norm of the equation residual as the coefficients a_{lm} are varied. This is a numerical minimisation problem in $\sim l^2_{max}$ variables.

The Nakamura method provides a direct iterative scheme for the coefficients a_{lm} and thus has certain computational advantages over the Eardley method. Only the coefficient a_{00} has to be determined as a root or a minimum. It has been shown that the Nakamura algorithm has exponential convergence (4.14) for the cases considered, and with suitable modifications (section 4.4), is robust and stable. The implementation of the algorithm does not present any special difficulties.

The Nakamura method, does however have certain disadvantages. The series formulation (3.40) implies that the method is computationally demanding if the marginally outer trapped surfaces are determined to high accuracy (4.17). The

method is thus unsuitable for the type of problem considered by Bishop (1984) where apparent horizons were determined for two black holes with a mass ratio $\frac{M_2}{M_1}$ as low as 10^{-6}.

The Nakamura method is very sensitive to the choice of initial trial solution, although this has been improved by making certain modifications to the algorithm (section 4.2c). Thus some prior knowledge of the position of the marginally outer trapped surface is required before using the algorithm. This method is thus not particularly suitable for finding highly distorted marginally outer trapped surfaces. This is confirmed by the failure to determine the surface S_2 (in Fig. 4.4) as found by Bishop (1982,1984) for the case of two Schwarzschild black holes.

It is also difficult to carefully control the region in which a search is conducted for trapped surfaces due to the iterative nature of the algorithm. This can be achieved in some limited sense by careful choice of the initial trial solution. The iteration can be slowed down by choosing the weighting factor $\Omega \ll 1$ in (4.16). It is not easy to carefully determine the closed trapped region using this method. Surfaces such as T_3 in Fig. 4.4 cannot be located using the Nakamura algorithm as they pass through a singularity.

The algorithm, however, does converge rapidly to smooth marginally outer trapped surfaces of the type S_{11}, S_{12} or S_3 in Fig. 4.4. In determining the outermost marginally outer trapped surface (i.e. the apparent horizon) it is usually adequate to choose a two-sphere centered at the coordinate origin and lying in the asymptotically flat region of the data surface as the initial trial solution. The apparent horizon is the most important marginally outer trapped surface. It is this surface that determines the efficiency limits for gravitational radiation and the point at which a black hole forms in the numerical evolution of the initial data.

It is also important to choose the origin of the spherical polar coordinate sys-

tem with care. Sensible choices are usually suggested by the phyical structure of the problem. If the origin is chosen too far off-centre for a distorted marginally outer trapped surface, the spherical polar coordinates may not cover the surface adequately.

As discussed in section 4.3, the algorithm could be improved in computational efficiency by various means. This would further improve the usefulness of the method.

In summary, the modified Nakamura algorithm is a good method of determining smooth marginally outer trapped surfaces in full (3+1) numerical relativity. The method should, however, be used with due consideration to the limitations mentioned above. A good a priori estimate of the apparent horizon is important for this method.

CONCLUSIONS

This research report has considered the problem of determining apparent horizons in (3+1) numerical relativity. A review has been provided of the initial value problem for black hole systems and the existing methods for solving the trapped surface equation. In particular, the method of Nakamura, Kojima and Oohara (1984) has been numerically evaluated and compared with the results of previous work which used different numerical methods.

The first example considered was that of a shifted Schwarzschild black hole. This requires the full (3+1) formalism and has a known analytic solution.

The algorithm was found to be very sensitive to the initial trial solution. In addition, the method diverged when attempting to determine some distorted marginally outer trapped surfaces. These difficulties were largely overcome by introducing several modifications to the algorithm. In particular, the procedure for determining the coefficient $a_{00}^{(n)}$ was made more robust by accepting minima as well as roots in the equation $\int_0^{2\pi}\int_0^{\pi} F_{00}\, d\Omega = 0$ (4.19), using current coefficients $a_{lm}^{(n)}$, $l, m \neq 0$ rather than coefficients from the previous iteration, and constraining $a_{00}^{(n)}$ such that the condition $r(\theta,\phi) > 0$ is enforced. The convergence of the algorithm was improved by introducing a weighted average of coefficients over successive iterations (4.16).

The algorithm was found to converge exponentially (4.14) and to require a computational effort of order $\sim O(\frac{1}{\epsilon^4})$ to achieve an accuracy ϵ in the marginally outer trapped surfaces. Various methods are proposed in section 4.3 to reduce the computational complexity of the algorithm. The modified Nakamura method was found to be robust and stable.

This method was applied to the case of two time-symmetric Schwarzschild black holes described by the Misner and Wheeler (1957) initial data. The results of Cadez (1974) and Bishop (1982), who determined apparent horizons for these initial data using different numerical methods, were confirmed with the exception that a distorted marginally outer trapped surface (S_2 in Fig. 4.4) was not found. The same system was also considered using inversion symmetric initial data (Misner 1963) and the results of Smarr et al. (1976) were confirmed.

The Nakamura algorithm was also applied to the case of three time-symmetric Schwarzschild black holes described by the Misner and Wheeler initial data. The black holes were collinear and equally spaced. The maximum efficiency for extracting gravitational wave energy from this system was determined as a function of coordinate separation. At the critical spacing $a_c \sim 1.5$, at which an apparent horizon forms enclosing all three black holes, the efficiency was found to be $\eta \sim 1.2$ x 10^{-2}. This is similar to the result obtained by Oohara, Nakamura and Kojima (1985) for three Schwarzschild black holes in an equilateral triangular configuration. The method could not be tested for black hole systems with non-zero linear and angular momentum as these initial data are not yet available (York 1988).

A discussion of the general applicability of the method is given in section 4.7. In summary, the method is well suited to determining the position of smooth marginally outer trapped surfaces. The algorithm has good convergence and is stable and robust. The method is not however suitable for determining apparent horizons to high accuracy (such as the work of Bishop (1984)) or the position of highly distorted marginally outer trapped surfaces. It is not easy to control the region in which a search is conducted for trapped surfaces and the method is thus not suited to determining the closed trapped region accurately. For initial data that have axial spatial symmetry, the method of Cadez (1974) and Bishop (1982) is superior.

There are several ways in which this research could be extended. The Nakamura method would be a very good technique for determining the apparent horizon of a Bowen-York black hole. It is not known whether the apparent horizon for this system would appear Lorentz contracted or not. The method could also be used to investigate the efficiency of energy extraction from magnetized black holes (Wagh, Dhurandhar and Dadhich 1985), which is of great astrophysical interest.

The algorithm could be improved numerically in various ways. Reducing the computational complexity of the algorithm using the techniques proposed in section 4.3 would be particularly useful. Other methods for solving the trapped surface equation could also be investigated, including finite difference schemes. This would, however, involve some linearisation of the equation.

REFERENCES

Adler, R., Bazin, M., and Schiffer, M., 1975, *Introduction to General Relativity, McGraw-Hill Kogakusha, Tokyo.*

Bishop, N.T., 1982, *Gen. Rel. Grav.*, **14**, 717.

Bishop, N.T., 1984, *Gen. Rel. Grav.*, **16**, 589.

Bishop, N.T., 1988, *Gen. Rel. Grav.*, **20**, 573.

Bowen, J. M., 1979, *Gen. Rel. Grav.*, **11**, 227.

Bowen, J. M., and York, J. W., 1980, *Phys. Rev. D*, **21**, 2047.

Bowen, J., Rauber, J., and York, J. W., 1984, *Class. Quantum Grav.*, **1**, 591.

Bowen, J. M., 1984, *J. Comp. Phys.*, **56**, 42.

Bowen, J. M., 1985, *Ann. Phys. (N.Y.)*, **165**, 17.

Brill, D. R., and Lindquist, R. W., 1963, *Phys. Rev.*, **131**, 471.

Centrella, J. M., Shapiro, S. L., Evans, C. R., Hawley, J. F., and Teukolsky, S. A., 1986, *in Dynamical Space-Times and Numerical Relativity, ed. J. M. Centrella, (Cambridge University Press, Cambridge).*

Cadez, A., 1974, *Ann. Phys. (N.Y.)*, **83**, 449.

Chandrasekhar, S., 1983, *The Mathematical Theory of Black Holes, Oxford University Press, Oxford.*

Davis, P. J., and Rabinowitz, P., 1975, *Methods of Numerical Integration, Academic Press Inc., London.*

Demianski, M., 1985, *Relativistic Astrophysics, Pergamon Press, Oxford.*

Eardley, D. M., 1978, *in Sources of Gravitational Radiation, ed. L. Smarr, (Cambridge University Press, Cambridge).*

Einstein, A., and Rosen, N., 1935, *Phys. Rev.*, **48**, 73.

Eppley, K., 1977, *Phys. Rev. D*, **16**, 1609.

Fletcher, C. A. J., 1984, *Computational Galerkin Methods, Springer- Verlag, New York.*

Flugge, S., 1974, *Practical Quantum Mechanics, Springer-Verlag, Berlin.*

Gibbons, G. W., 1972, *Comm. math. Phys.*, **27**, 87.

Gibbons, G. W., and Schutz, B. F., 1972, *M.N.R.A.S*, **159**, 41p.

Gradshteyn, I. S., and Ryzhik, I. M., 1980, *Table of Integrals, Series, and Products, Academic Press. Inc., London.*

Hawking, S. W., 1972a, *in Black Holes, eds. C. DeWitt and B. S. DeWitt, (Gordon and Breach Scientific Publ., New York).*

Hawking, S. W., 1972b, *in Black Holes: Selected Reprints, ed. S. Detweiler, (American Association of Physics Teachers, S.U.N.Y, New York).*

Hawking, S. W., and Ellis, G. F. R., 1973, *The Large Scale Structure of Space-Time, Cambridge University Press, Cambridge.*

IMSL Library Reference, 1987, *IMSL MATH/LIBRARY, Houston, USA.*

Kramer, D., Stephani, H., MacCallum, M., and Herlt, E., 1980, *Exact Solutions of Einstein's Field Equations, (Cambridge University Press, Cambridge).*

Kulkarni, A. D., Shepley, L. C., and York, J. W., 1983, *Phys. Lett.*, **96A**, 228.

Kulkarni, A. D., 1984, *J. Math. Phys.*, **25**, 1028.

Lindquist, R. W., 1963, *J. Math. Phys.*, **4**, 938.

MacCallum, M. A. H., 1986, *in Dynamical Space-Times and Numerical Relativity, ed. J. M. Centrella, (Cambridge University Press, Cambridge).*

Misner, C. W., and Wheeler, J. A., 1957, *Ann. Phys. (N.Y.)*, **2**, 525.

Misner, C. W., 1960, *Phys. Rev.*, **118**, 1110.

Misner, C. W., 1963, *Ann. Phys. (N.Y.)*, **24**, 102.

Misner, C. W., Thorne, K. S., and Wheeler, J. A., 1973, *Gravitation, W.H. Freeman and Compnay, San Francisco.*

NAG Library Manual, 1982, *Numerical Algorithms Group, Oxford.*

Nakamura, T., Kojima, Y., and Oohara, K., 1984, *Phys. Lett.*, **106A**, 235.

Newman, E. T., and Penrose, R., 1962, *J. Math. Phys.*, **3**, 566.

O'Murchadha, N., and York, J. W., 1974, *Phys. Rev. D*, **10**, 428.

Oohara, K., Nakamura, T., and Kojima, Y., 1985, *Phys. Lett.*, **107A**, 452.

Patterson, T. N. L., 1968, *Maths. Comp.*, **22**, 847.

Piessens, R., deDoncker-Kapenga, E.,Uberhuber, C. W., and Kahaner, D. K., 1983, *QUADPACK, Springer-Verlag, New York.*

Press, W. H., Flannery, B. P., Teukolsky, S. A., and Vetterling, W. T., 1987, *Numerical Recipes, Cambridge University Press, Cambridge.*

Quinn, M.J.,1988, *Designing Efficient Algorithms for Parallel Computers, McGraw Hill, Singapore.*

Rauber, J. D., 1986, *in Dynamical Spacetimes and Numerical Relativity, ed. J. M. Centrella, (Cambridge University Press, Cambridge).*

Sachs, R. K., 1964, *Relativity, Groups and Topology, eds. C. DeWitt and B. DeWitt, (Gordon and Breach Science Publishers, New York).*

Sasaki, M., Maeda, K., Miyama, S., and Nakamura, T., 1980, *Prog. Theor. Phys.*, **63**, 1051.

Schutz, B. F., 1986, *in Dynamical Space-Times and Numerical Relativity, ed. J. M. Centrella, (Cambridge University Press, Cambridge).*

Shapiro, S. L., and Teukolsky, S. A., 1979, *Ap. J.*, **234**, L177.

Shapiro, S. L., and Teukolsky, S. A., 1980, *Ap. J.*, **235**, 199.

Smarr, L., Cadez, A., DeWitt, B., and Eppley, K., 1976, *Phys. Rev. D*, **14**, 2443.

Smarr, L., and York, J. W., 1978, *Phys. Rev. D*, **17**, 2529.

Stephani, H., 1982, *General Relativity, Cambridge University Press, Cambridge.*

Wagh, S. M., Dhurandhar, S. V., and Dadhich, N., 1985, *Ap. J.*, **290**, 12.

Wald, R. M., 1984, *General Relativity, Univ. of Chicago Press, Chicago.*

York, J. W., 1973, *J. Math. Phys.*, **14**, 456.

York, J. W., 1978, *in Sources of Gravitational Radiation, ed. L. Smarr, (Cambridge University Press, Cambridge).*

York, J. W., and Piran, T., 1982, *in Spacetime and Geometry, eds. K. Matzner and L. Shepley, (Univ. of Texas Press, Austin).*

York, J. W., 1984, *Physica*, **124A**, 629.

York, J. W., 1988, *private communication.*